Surface-Initiated Polymerization Carbon Substrate: Polymer Brush Optimization and Adsorption of Naphthenic Acids in OSPW

A Thesis Submitted to the Committee on Graduate Studies in Partial Fulfillment of the Requirements for the Degree of Master of Science in the Faculty of Arts and Science

TRENT UNIVERSITY

Peterborough, Ontario, Canada

Materials Science M.Sc. Graduate Program

January 2026

Abstract

Surface-Initiated Polymerization on Carbon Substrate: Polymer Brush Optimization and Adsorption of Naphthenic Acids in OSPW

Teagan A. Carr

This thesis presents the design, synthesis, and evaluation of activated carbon polyacrylamide (AC-PAM) composites for oil sands tailings remediation, integrating flocculation and adsorption functionalities. Surface-initiated atom transfer radical polymerization (SI-ATRP) was employed to graft high molecular weight PAM brushes onto petroleum coke and commercial activated carbon, with SARA-ATRP yielding the most uniform architecture ($M_n \approx 5.2$ kg/mol, $Đ \approx 1.25$). Flocculation tests using mature fine tailings (MFT) revealed superior sedimentation and dewatering with SARA-ATRP composites, outperforming conventional PAM at lower dosages. Adsorption studies using benzoic acid and model naphthenic acids showed selective uptake governed by polymer brush morphology and molecular structure, with Dubinin–Radushkevich isotherms best capturing the behavior of ARGET-ATRP composites. Post-flocculation assays confirmed reduced metal and polymer contamination, validating dual-function efficacy. These findings underscore petcoke's viability as a sustainable substrate and highlight controlled polymerization as a critical driver for tuning composite performance in industrial water treatment.

Keywords

Activated carbon, polyacrylamide, grafting, atom transfer radical polymerization, mature fine tailings, flocculation, adsorption, isotherms

Acknowledgements

I would like to sincerely thank my supervisor, Dr. Andrew J. Vreugdenhil, for his unwavering support, guidance, and patience throughout the completion of my thesis. The past few years have been an invaluable learning experience, and I am deeply grateful for the opportunity to work under his mentorship. I extend my special thanks to Oliver Strong and Dr. Tyler Roy for their expert advice, technical assistance, and ongoing encouragement during my research. I am also grateful to all members of the Trent Inorganic Materials Research Laboratory - Kyle Fisher, Elmira Nazari, Hamant France, Kyle Reyes, Nethma Dissanayake, Tate Mazurkewich - for their camaraderie and support. My thanks also go to Paul Pede of Carbonix Inc. for his generous support throughout this work. I would like to acknowledge my committee members, Dr. Olena Zenkina and Dr. Kate Stewart, and Dr. Michael Katz for their insightful feedback and valuable contributions. Finally, I am profoundly thankful to my family for their unwavering support despite the distance, and to my friends for providing encouragement and a sense of belonging while I was far from home.

Contents

List of Figures

List of Tables

List of Abbreviations and Symbols

Abbreviations

AC	Activated Carbon
APS	Ammonium Persulfate
ARGET	Activators Generated by Electron Transfer
ATRP	Atom Transfer Radical Polymerization
BA	Benzoic Acid
BE	Binding Energy
BiBB	α-bromoisobutyryl bromide
DMAP	4-dimethylaminopyridine
DPA	Diphenylacetic acid
EBiB	ethyl α-bromoisobutyrate
ECP	ethyl 2-chloropropionate
GPC	Gel Permeation Chromatography
H_2SO_4	Sulfuric Acid
ICAR	Initiator for Continuous Activator Regeneration
KOH	Potassium Hydroxide
LC	Liquid Chromatography
Me_6TREN	tris[2-(dimethylamino)ethyl]amine
MFT	Mature Fine Tailings
M_W	Molecular Weight
NA	Naphthenic Acid
OSPW	Oil Sands Process-Affected Water
PAM	Polyacrylamide
Petcoke	Petroleum Coke
PMDETA	N,N,N’,N”,N”-pentamethyldiethylenetriamine
RAFT	Reversible Addition-Fragmentation chain Transfer
RDRP	Reversible-Deactivation Radical Polymerization
RID	Refractive Index Detector
SA	Succinic Acid
SARA	Supplemental Activator and Reducing Agent

SEC	Size Exclusion Chromatography
SET-LRP	Single-Electron Transfer-Living Radical Polymerization
SI	Surface Initiated
STEM	Scanning Transmission Electron Microscopy
TEA	Triethylamine
TEABr	triethylammonium bromide
TEM	Transmission Electron Microscopy
TGA	Thermogravimetric Analysis
THF	Tetrahydrofuran
TOC	Total Organic Carbon
VOC	Volatile Organic Compounds
XPS	X-Ray Photoelectron Spectroscopy

Symbols

Đ	Dispersity
Pn·	Propagating radicals
X	Persistent radical
Rp	Rate of polymerization
[M]	Monomer concentration
kp	Propagation rate constant
[M]0	Monomer concentration at time 0
[M]t	Monomer concentration at time t
kpapp	Apparent propagation rate constant
[P·]	Propagating radicals' concentration
Mn	Number average molecular weight
[I]0	Initiator concentration at time 0
[I]	Initiator concentration and dormant chain ends
[D]	Deactivator concentration
Pn-X	Dormant species in the form of an initiating alkyl halide
Cu(I)L	Transition metal complex in their lower oxidation state
kact	Activation rate constant
L	Ligand
Cu(II)L-X	Transition metal in its higher oxidation state coordinated with the
kdeact	halide ligand from the dormant species
KATRP	Deactivation rate constant
KET	Equilibrium constant for the electron transfer between the metal
KX	complexes
KEA	Equilibrium constant for the heterolytic cleavage of the Cu(II)L-X
KBD	bond

Ve	Equilibrium constant for the bond dissociation energy of the
Vi	propagating chain end and Alkyl halide initiator
Vp	Weight average molecular weight
Kd	Analyte's elution (retention) volume
V0	Interstitial volume of the column
n0	Pore volume of the packing
n’	Distribution coefficient
c	Void volume
Ni	Refractive index of the solvent
Mn, theo	corresponding to l = 0, 1, 2, …, n – 1, and j is the total angular
[M]0/[I]0	momentum
M_n, exp	Molecular weight of a chain
M_W, exp	Number of chains of a specific molecular weight
χ^2	adjusted chi-square
RMSE	Root mean square error
Akaike Information Criterion	AIC_c

1. Introduction

1.1 Flocculation of Mature Fine Tailings

The environmental risk associated with tailing ponds comes in part from volatile organic compounds (VOCs) released from the ponds into the atmosphere.[4] These emissions raise concerns about air quality and their broader ecological impact. The seepage of oil sands process-affected water (OSPW) into groundwater further complicates the situation. OSPW contains elevated concentrations of naphthenic acids (NAs), metals, and other dissolved compounds, which, if left unchecked, could lead to widespread contamination in the region surrounding the oil sands operations, with acute toxicity leading to death of most fish and invertebrates at a concentration ranging up to 100 ppm.[4–6] The growing inventory of tailings ponds in Alberta already covers more than 400 km², making it critical to manage these ponds effectively to minimize their long-term environmental impact.[1,5]

1.1.1 Fine Tailings

MFT typically contain 30-35 % solids, including bitumen, clays, and sands, and 65-70 % water.[1,7] The bitumen recovery process, despite its efficiency (88-95 % recovery rates), leaves behind significant amounts of residual organic material and fine particles that accumulate in tailings ponds.[1,7] The fine clays and silts in MFT settle extremely slowly, and the persistent electrostatic repulsion among the negatively charged clay particles exacerbates the issue.[8] This stabilization, compounded by the alkaline pH of the water in tailings ponds, causes the MFT to remain suspended for years, leading to the need for long-term storage solutions. Despite efforts, the oil sands industry continues to face significant challenges in

managing MFTs. Current dewatering technologies capable of recovering only around 70 % of the water from tailings, 3.3 cubic meters of tailings are still generated for every cubic meter of bitumen extracted.[9] As a result, there is a pressing need to improve existing technologies and develop new methods for effective water recovery and tailings consolidation.

Current research focuses on improving the removal of NAs in MFT ponds and developing more effective treatments to improve flocculation, adsorption, and water filtration.[10,11] Some emerging methods which break down these harmful organic compounds into less toxic substances include chemical oxidation, and biological treatment, where microorganisms are used to degrade NAs.[4,11] Advanced water treatment processes are also being explored to lower NA concentrations in tailings water before it is recycled or discharged. These innovations aim to address the limitations of current technologies and reduce the long-term environmental risks posed by MFT.

1.1.2 Flocculation Mechanism

In industries like oil sands mining, where mature fine tailings (MFT) are a byproduct of bitumen extraction, effective flocculation is crucial for managing waste and recovering water. MFT consists of fine clays, sand, water, and residual bitumen, and it remains in a gel-like state due to the high-water retention and slow settling of fine clay particles.[7] To accelerate the settling process, flocculants like polyacrylamide (PAM)-based polymers are used to aggregate the fine particles. However, commercial flocculants, originally designed for other applications, often result in the formation of loosely packed flocs with high water content. These flocs still require containment in tailings ponds and hold large volumes of water that cannot be recycled, posing both

environmental and operational challenges.[12,13] Current research focuses on optimizing flocculation techniques to enhance dewatering and water recovery from oil sands tailings. For example, treatments combining coagulants and flocculants are explored to overcome the repulsive forces between particles and promote aggregation more effectively. Coagulants like gypsum can reduce the electrostatic repulsion between particles, allowing the flocculants to form stronger, more stable flocs.[14,15] Despite these advances, the search for more efficient flocculants tailored specifically for oil sands tailings is ongoing. Ideally, such flocculants would form denser flocs with less water retention, facilitating more effective water recovery and reducing the environmental footprint of tailings ponds.[16,17]

Flocculation is a widely used method for separating fine particles from liquids, essential in various industries such as wastewater treatment, oil sands mining, and mineral processing. The process involves the aggregation of fine particles suspended in a colloidal solution, forming larger clusters called "flocs" that are easier to separate through sedimentation or filtration.[14,18,19] The primary driving force behind flocculation is the introduction of high molecular weight polymers, which act as bridges between particles, neutralizing their repulsive forces and promoting aggregation.[20,21] This process improves the sedimentation of solids, making it essential for managing waste materials like MFT in oil sands mining.

Figure 1: Bridging of clay particles via neutral polymers, where 1/k represents the Debye length (left). In lab flocculation (right).

In colloidal suspensions, particles often carry a negative surface charge due to their surface functionality, such as clay or mineral particles.[7,15,20] This charge attracts counter-ions from the surrounding solutions, forming an electrical double layer around each particle. The repulsive forces between these similarly charged particles prevent natural aggregation, keeping the suspension stable. Flocculation aims to overcome these repulsive forces, allowing particles to aggregate into larger clusters. Two primary mechanisms contribute to the destabilization of colloidal suspensions: bridging flocculation and charge neutralization.[18,22] Both mechanisms rely on the adsorption of polymers or polyelectrolytes onto the surface of particles, although the specific interaction depends on the nature of the polymers and particles involved.

Bridging flocculation occurs when long-chain polymers adsorb onto particle surface through van der Waals forces, hydrogen bonding or electrostatic attraction. Once adsorbed, the polymer chains extend into the surrounding solution as loops and tails, if these chains are long enough to extend beyond the particle's electrical double layer (1/k) , they begin to form polymer "bridges" between them.[23] The success of

bridging flocculation depends on several factors, including the size and concentration of both the particles and the polymers, the mixing conditions, and the viscosity of the suspension.[20,21,23] The effectiveness of this process depends on factors such as particle size and concentration, mixing conditions, and suspension viscosity. In concentrated colloidal systems, frequent collisions accelerate polymer adsorption, allowing extended chains to link multiple particles together.

Polyacrylamide (PAM) based flocculants are among the most commonly used polymers for bridging flocculation, especially in industries like oil sands mining.[24,25] PAM polymers are favored because they are water-soluble and can be synthesized with high molecular weights, which are critical for effective bridging.[18,21] The polymer chains need to be long enough to adsorb onto multiple particles, forming stable flocs. However, there is an optimum polymer dosage for efficient flocculation. If too much polymer is added, particles may become oversaturated with polymer, leading to a high surface adsorption density. This prevents the polymer from bridging between particles, resulting in poor flocculation performance. Beyond dosage sensitivity, PAM-based flocculants face additional challenges that motivate the search for improved materials. These include limited selectivity for specific particle types, poor performance in highly saline or high-pH environments, and low efficiency in tailings with ultrafine particles, where bridging is more difficult. Moreover, traditional PAM is typically non-biodegradable and may raise environmental concerns due to its persistence in aquatic systems. To address these issues, researchers are investigating modified PAM derivatives, grafted copolymers, and hybrid materials that combine PAM with functional components designed to enhance adsorption, improve stability under harsh conditions, and reduce environmental impact.

1.2 Petroleum Coke to Activated Carbon

Petroleum coke (petcoke) is a carbon-rich byproduct of the oil refining process, specifically produced during the extraction of bitumen from oil sands. It is particularly abundant in regions like Alberta, Canada, where large stockpiles are generated annually. As of December 2018, 9.5 Mm^3 of refined petcoke had been collected.[26] It is known for its high carbon content, low volatile compounds, and minimal ash content, making it an attractive, low-cost feedstock for producing activated carbon (AC). Due to the growing stockpiles of petcoke and the environmental and economic challenges they pose, there is significant interest in finding practical applications for this material. One of the most promising opportunities lies in transforming petcoke into activated carbon, which can serve as a valuable adsorbent in environmental applications such as wastewater treatment. Raw petcoke has limited porosity and requires chemical or physical activation to achieve the high porosity and surface area characteristic of efficient adsorbents.[27]

AC derived from petcoke has demonstrated excellent adsorption properties, including high porosity, large surface area (ranging from 800 to 1500 m^2/g), and a wide variety of functional groups.[28] These attributes make petcoke-sourced AC highly effective for removing organic pollutants such as naphthenic acids (NA's) and toxic heavy metals contaminants from polluted groundwater and industrial wastewater. The activation process typically involves chemical treatment with potassium hydroxide (KOH), a well-established method for increasing the surface area and developing a porous structure in carbon materials.[29] Furthermore, the presence of functional groups such as oxygen, nitrogen, and sulfur, introduced during activation, which can significantly influence the material's chemical properties. These functional groups can

impart acidic, basic, or neutral behavior to the activated carbon, enabling selective adsorption of specific contaminants, such as heavy metals and organic pollutants.

1.3 Polymer Brushes

Among various surface modification techniques, polymer grafting has gained significant attention for its ability to tailor the chemical and physical properties of substrates. This adaptability has led to the use of polymer grafting on a wide variety of substrates, including graphene, carbon nanotubes, metals, metal oxides, and even biological proteins. Polymer-modified activated carbon stands out as a particularly versatile material due to its tunable surface properties, which can improve surface wettability, colloidal and thermal stability, and adsorption capacities.[30–32] The covalent attachment of polymer chains to the surface forms what are commonly referred to as polymer brushes, which are valued for their dense coverage and customizable properties. Polymer brushes can be formed through three primary approaches: grafting-to, grafting-from, and grafting-through.[33,34] In the grafting-to method, end-functionalized polymer chains react with a functionalized substrate. Although this technique is straightforward, it does not yield densely packed polymer brushes because of steric repulsion between polymer chains as they approach the surface. The resulting limited grafting density hinders the functional versatility of the surface. Additionally, physisorption between polymer chains and the substrate further complicates the formation of uniform polymer coverage.

The grafting-through method involves growing polymer chains from a surface functionalized with polymerizable groups. While this method can lead to polymer brush formation, it suffers from less control over chain length and grafting density.

Additionally, this method tends to produce non-grafted polymer chains in solution, which further limits its effectiveness compared to the grafting-from approach.[32,35]

In contrast, the grafting-from approach offers a more efficient route for creating dense polymer brushes. Here, polymer chains are grown directly from initiator sites that are covalently attached to the surface.[33,34] This bottom-up method, often referred to as surface-initiated reversible-deactivation radical polymerization (SI-RDRP), allows for precise control over the polymerization process, resulting in higher grafting densities and better control of the polymer chain length.[36] Surface-initiated reversible-deactivation radical polymerization techniques, including methods such as atom transfer radical polymerization (ATRP), RAFT polymerization, and nitroxide-mediated polymerization, provide a powerful platform for customizing the surface properties of AC or other substrates. The grafting-from method's ability to fine-tune the polymerization process makes it ideal for applications requiring uniform and high-density polymer brushes, such as in catalysis, sensor design, and adsorption technologies.[37,38]

Given the advantages of higher grafting density, controlled polymerization, and consistent polymer chain length, the grafting-from approach has become the preferred method for creating functional polymer brushes. This is particularly useful for modifying AC, where precise control over surface characteristics is essential for improving adsorption, stability, and overall performance in industrial and environmental applications.

1.4 Reversible-Deactivation Radical Polymerization (RDRP)

Reversible-Deactivation Radical Polymerization (RDRP), also known as controlled/living radical polymerization, is a versatile polymerization technique that allows for the synthesis of polymers with controlled molecular weights, narrow molecular weight distributions, and precise architectures. Traditional free radical polymerization techniques typically lead to a broad range of molecular weights due to the rapid termination and chain transfer reactions. RDRP overcomes these limitations by establishing a dynamic equilibrium between a low concentration of active (propagating) radicals and dormant species.[39–41] This dynamic system enables a more controlled growth of polymer chains, significantly reducing the occurrence of irreversible termination reactions. RDRP techniques provide several distinct advantages, including a controlled polymerization allowing for pre-determined degrees of polymerization (DP_n) with a low dispersity (Đ), and, long-lived polymer chains, that retain end functionalities.[42,43]

1.4.1 Atom Transfer Radical Polymerization (ATRP)

Among RDRP techniques, ATRP is one of the most widely used methods due to its versatility. ATRP operates through a dynamic equilibrium between propagating radicals and dormant species, facilitated by a transition metal catalyst, usually copper, in different oxidation states. This is mediated and enhanced using a ligand (L). The mechanism of ATRP begins with the activation of a dormant species (P_n-X, where P_n represents the polymer chain and X is a leaving group, often an alkyl halide) by the transition metal catalyst in its lower oxidation state (Cu (I)). This activation generates a radical species (P_m) and converts the metal catalyst into its higher oxidation state (Cu (II)). The radical can then propagate by reacting with the monomer to form a new

growing radical which will either continue the polymerization process or revert to the dormant state by undergoing a deactivation step with Cu (II), thus re-establishing equilibrium.

The equilibrium constant for ATRP (K_{ATRP}) is defined as the ratio of the rates of activation (k_{act}) to deactivation (k_{deact}), and the polymerization rate can be expressed mathematically.[44,45] The key equations governing the ATRP mechanism are as follows:

$$K_{ATRP} = \frac{k_{act}}{k_{deact}} = \frac{\left[X - \frac{Cu^{II}}{L}\right][P_m]}{\left[\frac{Cu^{I}}{L}\right][P_n - X]}$$

Equation 1: Equilibrium constant for ATRP. Specifically defining the rate constant required for activation must be less than the rate constant for deactivation.

The stability of the radical species and the efficiency of the catalyst in maintaining the active/dormant equilibrium are crucial to the success of ATRP, influencing the polymerization kinetics and resulting polymer properties. The primary features and advantages of ATRP, and by extension RDRP, include first-order kinetics: ATRP displays first-order kinetics, characterized by a rate of polymerization (R_p) that is dependent on the concentration of the monomer and the active radicals.[42] Where $\frac{-d[M]}{dt}$ represent the rate of monomer consumption over time, and k_p is the rate of polymerization. This allows for predictable polymerization behavior and more straightforward modeling of reaction kinetics.[45] This is shown in equation 2: [43]

$$R_p = -\frac{d[M]}{dt} = k_p[M][P_n^*]$$

Equation 2: Rate of propagation for ATRP.

When predicting M_W, the degree of polymerization (DP_n) can be precisely controlled by the initial ratio of monomer (M) to initiator (I) and can be expressed mathematically, allowing for the synthesis of polymers with desired molecular weights.[44,46]

$$DP_n = \frac{\Delta[M]}{[I]_0} = \frac{[M]_0}{[I]_0}\ x\ monomer\ conversion$$

Equation 3: Number average degree of polymerization for ATRP.

Due to the controlled nature of ATRP, polymers can be synthesized with specific architectures, including block copolymers, and brushes. This is achieved by pausing the polymerization and adding different monomers, allowing for the growth of distinct polymer blocks. The narrow molecular weight distribution resulting from ATRP allows to produce monodispersed polymers, which allows for uniformity in materials produced.

1.4.2 Types of Atoms Transfer Radical Polymerization

ATRP has evolved through various modifications that aim to enhance its efficiency, reduce its sensitivity to oxygen, and lower the required catalyst concentrations. The main types of ATRP include Activators Generated by Electron Transfer (ARGET), Supplemental Activator and Reducing Agent ATRP (SARA ATRP), ICAR ATRP (Initiator for Continuous Activator Regeneration ATRP), single-electron transfer-living radical polymerization (SET-LRP). A summary of these methods, mechanisms, advantages, and limitations can be seen in Table 1.

Table 1: Comparison of types of ATRP synthesis.[36,47–51,51–53]

Method	Catalyst	Activator/ Regenerator	Mechanism	Advantages	Limitations
ARGET-ATRP	Cu (II) (low concentration)	Reducing agent (e.g., ascorbic acid)	Chemical reduction of Cu (II) to Cu (I)	Low catalyst, oxygen tolerance, scalable	Needs excess reducing agent
ICAR-ATRP	Cu (II) (low concentration)	Radical initiator (e.g., AIBN)	Radical regeneration of Cu (I)	Low catalyst, simple setup	Unwanted radical side reactions
SARA-ATRP	Cu (0) + Cu (II)	Cu (0) as a reducing agent	Cu (0) reduces Cu (II) to Cu (I), supplemental activators	Highly controlled polymerization	Complex system with multiple Cu species
SET-LRP	Cu (0)	Single-electron transfer	Direct SET from Cu (0) to initiator, followed by disproportionation	Fast, highly efficient polymerization	Oxygen-sensitive, hard to control at times

Classic ATRP has a transition metal catalyst which is added in its lower oxidation state, Cu (I), to initiate polymerization.[54] It is sensitive to oxygen, which can oxidize the Cu (I) to Cu (II), leading to reduced control over the polymerization.[54] Typically, a higher concentration of copper catalyst (1,000 to 10,000 ppm) is needed to maintain the necessary equilibrium. [39,52,54]

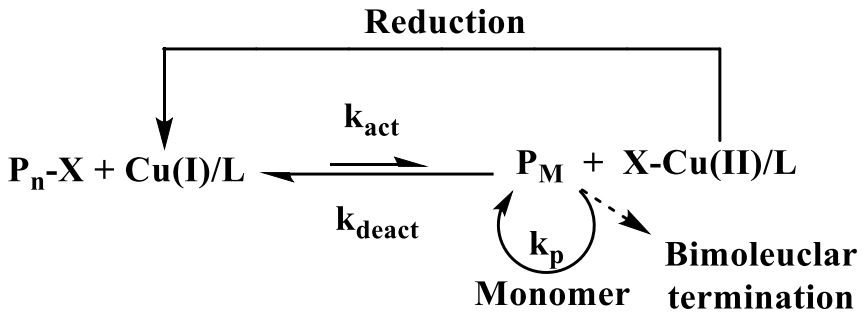

Figure 2: Mechanism of ATRP and ARGET-ATRP.

In contrast, ARGET ATRP enhances the oxygen tolerance of normal ATRP by utilizing a more oxidatively stable transition metal complex.[54,55] In this method, a chemical reducing agent (ascorbic acid) is added to generate the lower oxidation state catalyst in situ. This approach reduces the risk of oxidation of the catalyst, making the process more robust in the presence of oxygen. This allows for a significant reduction in catalyst concentration to less than 50 ppm.[51] By maintaining the Cu (I)/Cu (II) ratio through the continuous reduction of Cu (II) species back to Cu (I) using excess reducing agents, ARGET-ATRP demonstrates improved efficiency and therefore a greener approach to polymer synthesis.[56] The lower catalyst concentration is particularly advantageous for environmental and economic considerations. ICAR-ATRP employs a similar system where the activator (Cu (I)) is regenerated continuously during the polymerization process, enhancing control over the polymerization kinetics and allowing for higher polymerization rates and conversions.[57] This method is often characterized as a “reverse” ARGET-ATRP.[58]

On the other hand, SARA-ATRP is a newer technique that combines aspects of ATRP with RAFT, wherein the deactivation of growing radicals is controlled selectively, allowing for more intricate polymer architectures and functionalities. This is a more efficient method as it uses a zero-valent metal, typically copper (0), as a

reducing agent. The process still relies on the dynamic equilibrium which exists between an active Cu (I) species and a deactivator Cu (II) species; however, the Cu (0) to continuously reduce Cu (II) to Cu (I), maintaining the activator concentration and extending the "living" nature of the polymerization. In contrast, SET-LRP relies on a distinct outer-sphere electron transfer process. Polymerization is initiated by Cu (0), which disproportionation thus favouring polar solvents such as water. The Cu (II) formed acts as a deactivator, reversibly capping the growing radical chains and maintaining control over the polymerization process by minimizing termination events. Both methods utilize Copper (0) for polymerization. However, as seen in Figure 3, SARA-ATRP undergoes comproportionating (blue) whereas SET-LRP undergoes disproportionation (green). Both tend to be more controlled than traditional ATRP.

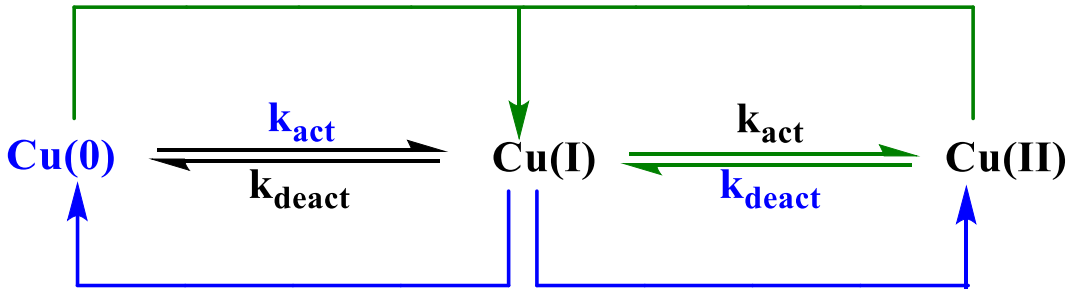

Figure 3: SARA-ATRP (blue) & SET-LRP (green).

1.5 Adsorption

Adsorption is an enthalpy driven, surface-based process in which molecules from a fluid phase accumulate on the surface of a solid adsorbent. It is widely employed for removing organic and inorganic contaminants from aqueous environments due to its simplicity, scalability, and efficiency. AC is one of the most

extensively used adsorbents due to its high surface area and chemical stability. It can be derived from low-cost feedstocks such as petroleum coke and biomass, making it especially attractive for large-scale applications. In the context of OSPW, AC has demonstrated high adsorption capacities, up to 400 mg/g for model NAs through mechanisms that include π-π stacking and hydrogen bonding.[28,29,59,60] Adsorption performance is typically assessed through equilibrium isotherm models, which describe how adsorbate molecules partition between the liquid phase and the adsorbent surface. Common models include the Langmuir isotherm, which assumes monolayer adsorption on a uniform surface; the Freundlich isotherm, which accounts for heterogeneous surface energies and multilayer adsorption; and the Sips isotherm, which combines both behaviors to describe complex adsorbents. Kinetic modeling, including pseudo-first-order, pseudo-second order, and intraparticle diffusion models, is equally important for identifying rate-limiting steps and understanding the dynamics of contaminant uptake over time.

Building on the effectiveness of AC, recent efforts have focused on creating composite materials that incorporate activated carbon into polymer matrices. Grafted polymers, such as functionalized polyacrylamides, can introduce additional binding sites or hydrophobic domains, while such composites are often designed for flocculation their adsorption potential remains under-characterized. The polymeric phase may alter adsorption kinetics through diffusion limitations or swelling effects and can significantly affect surface heterogeneity and binding affinity. Therefore, evaluating both isotherm and kinetic behavior is essential to fully understand the dual-function potential of polymer-AC composites for OSPW treatment. This work aims to explore these interactions, using model naphthenic acids to assess adsorption capacity and behavior as a function of molecular structure and composite design.

1.5.1 Modelling

Adsorption isotherms provide critical insights into the interactions between adsorbates and adsorbent surfaces, serving as fundamental tools to characterize adsorption phenomena under equilibrium conditions. The classical framework for understanding adsorption behaviors on solids is grounded in the Brunauer-Emmett-Teller (BET) classification, which categorizes isotherms into six distinct types based on their shape and the underlying physicochemical processes.[61]

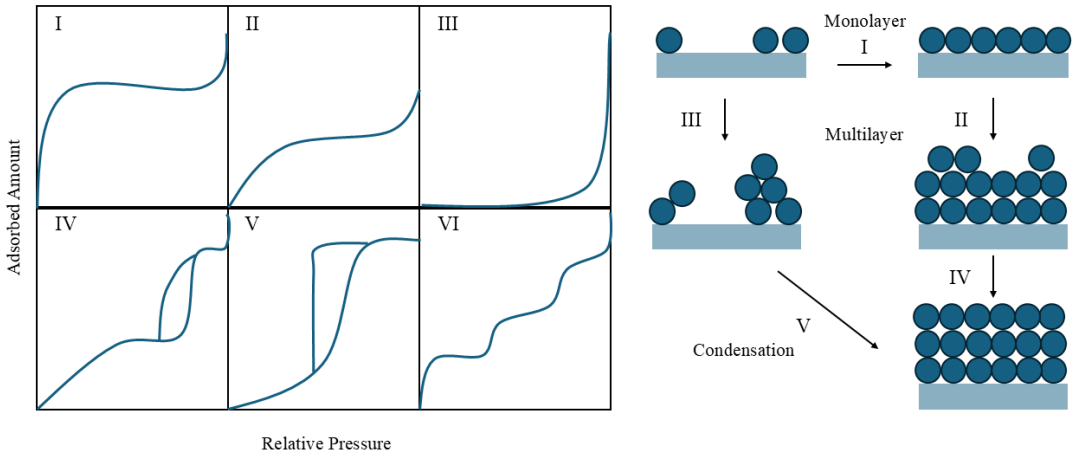

Figure 4: IUPAC classification of adsorption isotherms.

These categories reflect variations in adsorbate-adsorbent affinities, surface heterogeneity, pore structure, and intermolecular interactions among adsorbed species. Type I isotherms are characteristic of microporous solids undergoing monolayer adsorption. Type II and Type IV isotherms are often associated with non-porous or mesopores materials, representing multilayer adsorption mechanisms, with step IV displaying capillary condensation when the adsorbate is gaseous. S-shaped or sigmoidal isotherms (commonly related to Type III and Type V isotherms), indicate complex adsorption dynamics that cannot be adequately described by simple monolayer adsorption models such as Langmuir's.[62,63] The S-shaped isotherm reflects

a cooperative adsorption mechanism, where adsorbate-adsorbate interactions significantly enhance adsorption affinity at higher surface coverages, often due to cluster or multilayer formation, pore-filling effects, or adsorbate-induced surface restructuring.[63,64] This behaviour suggests the presence of energetically heterogeneous adsorption sites and highlights the importance of lateral interactions between adsorbed molecules, leading to sigmoidal isotherms.

Consequently, conventional models assuming uniform surface energy and independent adsorption sites are insufficient to capture such phenomena. Understanding and modeling S-shaped isotherms require more sophisticated approaches that incorporate these cooperative effects, such as the Sips isotherm, Redlich-Peterson (R-P) and Dubinin-Radushkevich (D-R), and related statistical mechanical models.[65,66] The R-P model interpolates between Langmuir and Freundlich behavior, providing flexibility for heterogeneous systems without assuming monolayer adsorption exclusively.[67] The D-R model emphasizes adsorption energy distribution and can help distinguish between physical and chemical adsorption mechanisms.[68,69] These models allow the quantification of adsorption capacity and affinity while accounting for surface heterogeneity and multilayer formation, making them highly relevant for complex adsorbents like activated carbon-polymer composites interacting with environmentally persistent compounds such as naphthenic acids. Therefore, a thorough investigation of S-shaped isotherms provides a more comprehensive understanding of adsorption mechanisms critical for optimizing materials and processes for contaminant removal in aqueous environments.

2. Key Experimental Techniques

2.1 Key Characterization Techniques

2.1.1 Size Exclusion Chromatography (SEC)

Understanding the molecular weight (M_W) of a polymers can help to understand it's relative properties. One of the most common methods used to determine molecular weights and their distributions is Size Exclusion Chromatography (SEC), also known as Gel Permeation Chromatography (GPC). SEC separates polymer molecules based on their size in solution, which is related to the hydrodynamic volume of the molecules rather than their molecular weight. By correlating the retention times of a specific polymer to the molecular weights through calibration, it is possible to derive important molecular weight parameters such as the Number Average Molecular Weight (M_n), Weight Average Molecular Weight (M_w), and Polydispersity Index (Đ).

The separation occurs as molecules pass through a column packed with a stationary phase composed of spherical beads containing pores of a defined size distribution. As molecules traverse the column, they are either included in or excluded from the pores, leading to differences in their elution volumes. Large molecules that cannot enter the pores of the beads will elute rapidly because they take the shortest path through the column. These molecules elute at the void volume (V_o), which represents the volume of the mobile phase outside the pores. Small molecules, which have access to the entire pore structure, will elute more slowly as they travel through both the pores and the mobile phase. These molecules elute at the total liquid volume (V_t), which is the sum of the void volume and the total pore volume (V_i). Molecules of intermediate size only penetrate some of the larger pores and will elute between V_o

and Vt. The elution volume (V_e) for these molecules is governed by how much of the internal pore volume they can occupy. This is described by

$$V_e = V_0 + K_{SEC}V_i$$

Equation 4: Elution volume of the analyte.

where K_{SEC} is the fraction of the internal pore volume accessed by the molecules. Large molecules that pass directly through the column without entering the pores have $K_{SEC} = 0$ ($V_e = V_o$), while small molecules that access the entire pore volume have $K_{SEC} = 1$ ($V_e = V_o + V_i$).

The number average molecular weight (M_n) is the average molecular weight of the polymer chains in the sample and is calculated by giving equal weight to each molecule, regardless of its size. The equation for M_n is

$$M_n = \frac{\sum N_i M_i}{\sum N_i}$$

Equation 5: Number average molecular weight.

Where N_i is the number of polymer molecules of molecular weight M_i in the sample. M_i are the molecular weights of individual polymer chains. In this formula, M_n is the total molecular weight of all molecules divided by the total number of molecules. M_n gives more importance to smaller molecules in the polymer sample because it counts each molecule equally, regardless of size.

The weight average molecular weight (M_w) takes into account not only the number of molecules but also their masses. It provides more weight to the larger polymer molecules, as their mass significantly contributes to the overall weight of the sample. M_w is calculated as

$$M_w = \frac{\sum N_i M_i^2}{\sum N_i M_i}$$

Equation 6: Weight average molecular weight.

Here, M_i^2 indicates the contribution of heavier molecules to the molecular weight average. Therefore, M_W tends to be higher than M_n unless the polymer is monodispersed, meaning all polymer chains have the same molecular weight.

The polydispersity index (Đ), denoted as Đ, is a measure of the breadth of the molecular weight distribution in the polymer sample. It is defined as the ratio of M_W to M_n:

$$Đ = \frac{M_w}{M_n}$$

Equation 7: Dispersity.

If Đ = 1, the polymer is perfectly monodispersed, meaning all polymer chains have the same molecular weight. Most synthetic polymers are polydisperse, meaning that their molecular weight distribution is broader and Đ > 1. The Đ gives insight into the uniformity of the polymer. For example, polymers synthesized by living polymerization techniques tend to have narrow molecular weight distributions (low Đ), whereas polymers made by free radical polymerization typically exhibit broader distributions (high Đ). Dispersity (Đ), or the polydispersity index, is calculated by determining both M_n and M_W from the SEC data. By integrating the detector signal over the elution volume, the weight fractions corresponding to each elution volume can be measured. These fractions are used to calculate M_n and M_W using the equations provided earlier.

In GPC the refractive index detector (RID) is typically used. This measures the difference in the refractive index between the mobile phase and the pure solvent held in a reference cell.

$$n = n_0 + (n' - n_0)c$$

Equation 8: Refractive index of a dilute solution.

Where n_0 is the refractive index of the solvent, n' is the sample's refractive index, and c is the concentration of the sample in solution. This equation can be rearranged to form.

$$c = \frac{n - n_0}{n' - n_0}$$

Equation 9: Concentration of the sample in solution.

Which demonstrates that the difference in the RI between solvents and the sample solution are proportional to the sample concentration.

The SEC column must be calibrated with monodisperse polymers with known peak molecular weights (M_p). The calibration of the column is achieved by taking a linear regression of the logarithmic plot of the standards M_n, and the elution volumes of their peak maxima. The molar mass distribution can be calculated using this calibration. The calibration standards should also be chemically like those of the analysed samples. The macromolecule's chemical composition, topology, solvent, and more affect the hydrodynamic volume of a polymer. Polyethylene oxide/polyethylene glycol standards are most often used to analyse aqueous linear polymers.

The molar mass and molar mass distributions in this work were determined by SEC using Agilent Technologies 1220 Infinity LC equipped with an Agilent

Technologies 1260 Infinity RID. The SEC column used was a PL aquagel-OH MIXED-H 8 µm, 300 x 7.5 mm column with a molar mass lower limit of 6000 g/mol and upper limit of 10,000,000 g/mol. The eluent was an aqueous solution of 0.2 M $NaNO_3$ and 0.01 M NaH_2PO_4 adjusted to pH 7 using 0.1 M NaOH. Samples were diluted to 0.1% (w/v %) and were injected at a volume of 20 µL. The column was operated at room temperature with a 1 mL/min flow rate while the detector was set at 35 °C. The column was calibrated using polyethylene oxide/polyethylene glycol standards with monodisperse molar mass distributions at Mn values in the 106 - 522,000 g/mol (Agilent Technologies).

2.1.2 X-Ray Photoelectron Spectroscopy (XPS)

X-ray Photoelectron Spectroscopy (XPS) is a surface characterization technique used to analyze the elemental composition, chemical state, and electronic state of elements present within a material. XPS operates on the principle of the photoelectric effect, wherein the surface of a material is irradiated with X-ray photons.[70] This irradiation causes the emission of electrons, known as photoelectrons, from the material. The fundamental process involves a complete transfer of energy from the X-ray photons to the inner shell electrons of the sample.[71] When an X-ray photon impinges on an atom, it provides enough energy to eject an inner shell electron, creating a "hole" in the electron's orbital.[70,71] This ejection leaves the atom in an excited state, which is then stabilized by filling the vacancy with an electron from a higher energy level. The relaxation of the atom can occur either by the release of energy as X-ray fluorescence or through the emission of an Auger electron.[71]

In XPS, the kinetic energy of the emitted photoelectrons is measured, which is directly related to the binding energy of the electrons in the atom. The relationship

between the kinetic energy of the photoelectrons and the binding energy can be described by the following equation:

$$E_k = hv - \Phi - BE$$

Equation 10: The Photoelectric effect.

Where E_k represents the kinetic energy of the emitted photoelectron, hv is the energy of the incident X-ray photon, and BE is the binding energy of the electron in the atom.[72,73] The work function is symbolized by Φ and is defined as the energy difference between the Fermi level and the vacuum level. The XPS analysis accounts for the energy required to extract an electron from the solid into the vacuum. By measuring the kinetic energy of the photoelectrons and knowing the photon energy and work function, the binding energy of the electrons can be calculated. This binding energy provides valuable information about the elemental composition and chemical state of the atoms in the material.

The XPS spectrum is constructed by plotting the intensity of the detected photoelectrons as a function of their binding energy. Each element in the sample produces characteristic peaks in the spectrum corresponding to different core levels, such as the 1s, 2s, or 2p levels.[72] Chemical shifts in binding energy can indicate oxidation states or changes in the chemical environment. These shifts occur due to variations in the electrostatic potential experienced by the electrons, which are influenced by the chemical bonding and local environment of the atoms.

Quantitative analysis in XPS involves integrating the area under each peak in the spectrum, which correlates to the concentration of the corresponding element. This analysis is performed by applying sensitivity factors and photoionization cross-

sections for the elements of interest. Sensitivity factors are empirical corrections that account for the variation in detection efficiency among different elements and their respective photoelectron escape depths.

Despite its powerful capabilities, XPS has certain limitations. Its primary focus is on the outermost layers of the material, typically probing only the top 1 to 10 nanometers.[71] This surface sensitivity is advantageous for analyzing thin films and surface treatments but may not provide sufficient information about deeper layers. To study the depth profile of a material, sputter depth profiling techniques can be employed, where the surface is sequentially removed using ion sputtering, and XPS measurements are taken at each depth. However, sputtering can alter the sample and introduce artifacts, so careful interpretation is required. In this thesis, XPS was employed to characterize surface functionality following oxidation and initiator attachment of AC, which provided insight into the chemical modification necessary for the subsequent polymerization.

2.2 Key Measurement Techniques

2.2.1 Flocculation Measurement Techniques

2.2.1.1 Dean Stark Extraction

The Dean-Stark extraction technique is used to analyze the composition of suspensions, such as mature fine tailings (MFT). Flocculation is a process where fine particles aggregate into a floc or a flake, which then settles out of the liquid. The performance of flocculants is highly dependent on the composition of the suspension, which includes the solid content, water content, and the presence of bitumen or other substances.

The technique relies on the principle of distillation and phase separation. In a Dean-Stark apparatus, the sample containing water is mixed with an organic solvent that is immiscible with water, such as toluene. As the mixture is heated, the solvent and water evaporate together, condense, and then separate due to their differing densities. This separation allows for the accurate measurement of water content. By using Dean-Stark extraction, researchers can precisely measure these components, ensuring consistent and accurate results in flocculation tests. This is crucial because variations in the composition of the suspension can significantly impact the efficiency of the flocculants and the overall flocculation process.

The procedure used to prepare samples starts by weighing approximately 12.5 grams of sample (e.g., MFT) and placing it in a pre-weighed thimble. The thimble is designed to hold the sample during the extraction process. The Dean-Stark apparatus includes a reflux flask, a condenser, a water trap, and the thimble holder. Around 200 mL of toluene is added to the reflux flask. Toluene acts as the organic solvent in this process. A thimble containing the sample is suspended above the reflux flask so that it hangs in the toluene. Heating the toluene subsequently initiates refluxing. As the toluene evaporates, it carries the water vapor from the sample. The vaporized toluene and water pass through the condenser, where they are cooled and condensed into a liquid. The mixture of condensed liquids then drips into the water trap. Due to the immiscibility of toluene and water, they separate into distinct layers, with toluene forming the top layer. The reflux continues for approximately 24 hours. This ensures that all the water and bitumen have been extracted from the sample. The process continues until the toluene dripping from the thimble is visibly free of bitumen. After the reflux is complete, the thimble is removed and dried at 110 °C overnight. Once dried, the mass of the thimble containing the residual solids in the sample is taken.

The water from the trap is drained and weighed to determine the amount of water extracted.

2.2.1.2 Settling Test

A settling test serves to evaluate how effectively solid particles in a suspension settle, which can be useful in various industries like wastewater treatment, mining, and chemical engineering. Specifically, settling tests involving flocculants are used to determine how quickly a flocculant, can cause solids in the suspension to settle. The goal is to assess the rate of sedimentation and the clarity of the liquid after settling. This is done through flocculant addition to the suspension (in this case, a slurry) with varying doses. The suspension is mixed thoroughly, typically at varying speeds to ensure even distribution of the flocculant. For example, in one test, a mixture of slurry and flocculant was stirred at 600 rpm for 2 minutes, followed by 200 rpm for 8 min. After mixing, the suspension is transferred to a graduated cylinder, where the settling behavior is observed. The key measurement is the mudline height, which represents the interface between the solid particles settling at the bottom and the clear liquid above. By recording how this height changes over time, a settling profile can be created.

The settling profile is a plot of mudline height versus time. The initial linear section of this profile, which corresponds to the rapid, early-stage settling of particles, is called the Initial settling rate (ISR). It provides insight into how quickly the flocculation process starts, giving a measure of the initial flocculation kinetics. In a specific test, 100 g of MFT slurry diluted to 5 % solids was used. The mixture was transferred to a 100 mL graduated cylinder after being thoroughly stirred. The change in mudline height was recorded over time to create the settling profile, and the ISR

was calculated as the slope of the initial linear part of this profile. After 24 hours, the liquid at the top, known as the supernatant, was collected for further analysis, including turbidity measurements.

The turbidity of the supernatant indicates how well the flocculant settled the fine suspended particles. Turbidity is measured using a DR/890 Portable Colorimeter through an attenuation method, where a light beam passes through the sample. The intensity of the light decreases due to scattering and absorption by particles in the sample, with results expressed in Formazin Attenuation Units (FAU). Lower turbidity indicates clearer water, implying that the flocculant was effective at settling the particles.

Combining the general settling test procedure with specific methods, such as adding a flocculant and measuring turbidity, helps provide a comprehensive understanding of particle settling dynamics, flocculation efficiency, and the quality of the separated liquid. This type of test is especially valuable for assessing the performance of flocculants in treating suspensions like MFT slurry.

2.2.2 Adsorption Measurements

2.2.2.1 Total Organic Carbon

Total Organic Carbon (TOC) analysis is a widely used instrumental technique for quantifying the overall organic carbon content in complex water samples. Although it is nonspecific, meaning it cannot distinguish between different organic compounds, it provides a cumulative measure of all organic species present. As a result, its utility in characterizing OSPW is limited. However, due to its simplicity, ease of operation, and broad applicability to organic compounds, TOC analysis is well-suited for evaluating individual model naphthenic acids. It requires minimal

method development and is ideal for processing the large number of samples generated in adsorption tests with model naphthenic acids.

A Shimadzu TOC-VCPH analyzer equipped with an AIS-V autosampler was used to assess all model naphthenic acid adsorption tests. The instrument operates by combusting samples at 680 °C in a chamber containing a platinum catalyst, converting organic carbon into CO_2. A filtered air carrier gas transports the combustion products to a non-dispersive infrared detector that quantifies the CO_2 generated. The analyzer supports multiple operational modes. For most model naphthenic acids, the non-purgeable organic carbon method was employed. This involves acidifying the sample and purging it with carrier gas to remove inorganic carbon, followed by sample injection into the combustion chamber. The resulting signal corresponds to the TOC content, which is quantified using a standard calibration curve.

2.2.2.2 Direct Injection Mass Spectroscopy

Mass spectrometry (MS) is a highly versatile analytical technique used across a broad range of scientific fields, including chemistry, biology, environmental science, pharmaceuticals, and materials science. Its primary function is to identify chemical species by measuring their mass-to-charge ratio (m/z), however, in this work it will be used for quantification. MS can be used to determine molecular structures, isotopic compositions, and elemental identities. At its core, mass spectrometry involves three main components, Ion Source - to convert analyte molecules into ions, mass analyzer - to detect/separate the ions present at each m/z ratio, and detector - to measure the abundance of each ion.

In the MS experiments, ionization was achieved through electrospray ionization (ESI) - a soft ionization method ideal for analysing large, polar, and

thermally fragile molecules. ESI works by applying a high voltage to a liquid sample, generating a fine aerosol of charged droplets. As the solvent evaporates, multiply charged ions are released into the gas phase with minimal fragmentation, allowing for intact molecular ions to be analysed. Once ionized, the charged species are accelerated by an applied electric potential (V), gaining kinetic energy. The velocity (v) of the ion can be derived from

$$v = \sqrt{\frac{2qV}{m}}$$

Equation 11: Velocity equation rearranged.

These ions then enter a magnetic field (B), oriented perpendicular to their motion. Here, they experience a magnetic force described by

$$F_c = qvB$$

Equation 12: Lorentz Force Law equation.

Because of the force provided by centripetal acceleration during circular motion, it can be equated with Newton's second law.

$$F_c = \frac{mv^2}{r}$$

Equation 13: Newton's second law for circular motion.

Setting Equation 12 equal to Equation 13 and substituting in Equation 11 we can account for the radius.

$$r = \sqrt{\frac{2mV}{qB^2}}$$

Equation 14: Radius of curvature of the ion.

This equation shows that the radius of the curvature of the ion's path is dependent on its mass-to-charge ratio, assuming a constant electric potential and magnetic field. Therefore, ions of different masses will follow different trajectories, enabling separation based on mass.

After mass separation, ions are directed into Faraday cups, which serve as sensitive detectors. When an ion strikes the metal surface of the cup, generates a small current proportional to the number of ions. This current is amplified and recorded, producing a mass spectrum, a plot of ion abundance versus m/z ratio. The entire process typically occurs under high vacuum to prevent ion scattering or energy loss due to collisions with gas molecules.

For this work, a Thermo Fisher QExactive Orbitrap mass spectrometer (San Jose, CA). a high-resolution, high-accuracy instrument ideal for measuring exact masses of polar and complex analytes. The Orbitrap analyser works by trapping ions in an electrostatic field where they oscillate along the axis of a central electrode. The frequency of these oscillations is proportional to the m/z of the ion, and through Fourier transform-based signal processing, highly accurate mass data can be extracted.

2.3 Adsorption Techniques

2.3.1 Batch Adsorption

Adsorption is a process in which contaminants are removed from solution by accumulating on the surface of a solid adsorbent. This process continues until the

adsorbent surface becomes saturated or the contaminant is completely removed from the solution. Initially, adsorption is rapid due to a high concentration gradient, but the rate gradually slows as the system approaches equilibrium. This occurs when the number of occupied adsorption sites balances with the contaminant concentration remaining in solution. Adsorption kinetics typically proceed through three main stages.[74] The first stage involves external diffusion, where contaminants migrate from the bulk solution to the outer surface of the adsorbent, driven by the concentration gradient. This is followed by internal diffusion through the adsorbent's porous structure, and finally, attachment of the adsorbate to available active sites on the absorbent. The final adsorption step may involve various mechanisms, including hydrogen bonding and electrostatic interactions.[10,75] A schematic representation of adsorbate transport within a porous adsorbent is shown in Figure 5.

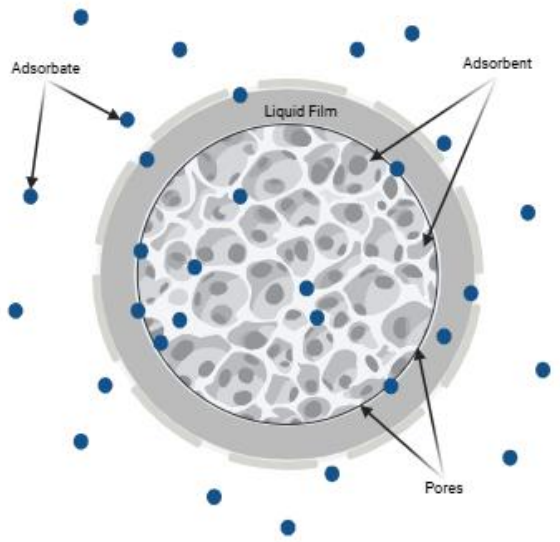

Figure 5: Schematic of adsorbate transportation through a porous adsorbent to adsorption sites.

Batch adsorption kinetic tests are often used to evaluate the time dependent adsorption behaviour of solution-based contaminants the material balance expression, to determine the adsorption capacities at each time point. For the kinetic evaluation of individual model NAs, an initial concentration of 60 ppm was used for all kinetic experiments throughout this thesis. The mass of adsorbent used was optimized for each adsorption system, and adsorption was evaluated up to 1-3 days. Mixing speeds were set to 250 rpm using a Thermo Scientific MaxQ 416 HP orbital shaker. All model NA solutions were buffered to a pH of 8 using an inorganic phosphate buffer to simulate the pH of real OSPW and all time points were evaluated in triplicate. 0.45 μm filter attached to a syringe was used to filter each batch sample so concentrations could be analyzed via TOC or MS analysis.

2.3.2 Adsorption Kinetics

Several kinetic models such as zero-order, first-order, second order, and multi-exponential (m-exp) models are commonly employed to gain insight into adsorption mechanisms and rates. Among these, the multi-exponential model was selected for this study due to its ability to capture the complexity and heterogeneity inherent in real-world systems. Unlike simpler models, the m-exp model accounts for multiple simultaneous adsorption processes occurring at different rates, making it more suitable for predicting and analyzing the dynamic behavior of structurally diverse contaminants in complex aqueous environments like OSPW.

The m-exp model is typically interpreted as a series of parallel pseudo-first-order processes, each representing a kinetically distinct adsorption pathway observed in experimental data.

$$q_t = q_e - q_e \sum_{i=1}^{n} f_i exp^{-k_i t}$$

Equation 15: m-exp model used for kinetic modelling.

where f_i is the fractional contribution of each kinetic phase, k_i is the corresponding rate constant (1/min), and the sum of all f_i values equals 1.[76] This equation serves as an empirical framework for describing adsorption kinetics and allows for the calculation of half-life times $t_{1/2}$, which indicate the time required for 50 % of adsorption to occur in each kinetic segment. These half-life values were subsequently used to compare the adsorption behaviour of different model naphthenic acids, providing a more nuanced understanding of how molecular structure influences adsorption rate across heterogeneous materials.

2.3.2 Adsorption Isotherms

Adsorption isotherms are another valuable type of batch test typically performed alongside kinetic studies to assess the maximum adsorption capacity of an adsorbent. These tests are critical for optimizing adsorption systems. Equilibrium in adsorption is a dynamic state influenced by both the quantity of adsorbent and the contaminant concentration in solution. Changes to either parameter shift the equilibrium, which forms the foundation of isotherm analysis. For model NAs, two main approaches are commonly used to generate isotherms, the variable mass method, where adsorbent dosage varies while contaminant concentration remains fixed, and the variable concentration method, where a constant adsorbent mass is exposed to varying initial contaminant concentrations. Both approaches are suitable, though some preliminary optimization is generally required to ensure accurate and complete isotherm data.

In this thesis, the variable mass method was used for all isotherm experiments. Adsorbent dosages were carefully optimized for each model NA based on an initial concentration of 60 mg/L. Mixing times ranged from 24 to 360 hours, depending on the adsorbent, to ensure that equilibrium was reached. All experiments were conducted in triplicate, using consistent solution volumes and mass-to-volume ratios, and buffered at pH 8. Adsorption isotherms are presented as the equilibrium adsorption capacity (q_e) plotted against

2.2.2.1 Langmuir

Initially developed to describe the adsorption of gases onto solid surfaces, the Langmuir isotherm model has since been extensively applied to a wide range of liquid-phase adsorption systems, including the treatment of contaminated aqueous solutions.[77] The model is predicated on a series of idealized assumptions that (a) adsorption occurs at discrete and energetically equivalent sites on the adsorbent surface, (b) each site accommodates only one adsorbate molecule, resulting in monolayer coverage, (c) there are no interactions between adsorbed species on adjacent sites, and (d) the energy of adsorption is invariant with surface coverage, implying a structurally and chemically homogeneous surface.

$$q_e = \frac{Q_0 K_L C_e}{1 + K_L C_e}$$

Equation 16: Langmuir isotherm modelling equation.

In Equation 1, Q_0 (mg/g) and K_L (L m/g) are representative of the monolayer saturation capacity and the Langmuir constant respectively. K_L is directly related to the adsorbate affinity to an adsorbents surface, The Langmuir constant K_L reflects the

affinity of the adsorbate for the surface, where a larger K_L implies a more negative Gibbs free energy, meaning adsorption is more favorable.[78]

2.2.3.2 Freundlich

The Freundlich isotherm model, a modelling equation commonly employed in adsorption studies, is particularly describing adsorption onto heterogeneous surfaces. Unlike the Langmuir model, the Freundlich isotherm does not assume monolayer coverage or uniform adsorption energies. Instead, it accounts for the non-uniform distribution of adsorption heat and affinities across the surface and allows for the possibility of multilayer adsorption. As such, it is frequently applied to systems where the surface complexity of the adsorbent precludes idealized behavior.

$$q_e = K_F {C_e}^{n^{-1}}$$

Equation 17: Freundlich isotherm modelling equation.

In Equation 17, K_F ((mg/g)/(L m/g)$^{1/n}$) is the Freundlich constant describing the strength of adsorption.[79] The parameter 1/n is dimensionless, and its magnitude offers insight into the nature of the adsorption process. Values of 1/n between 0 and 1 indicate favorable adsorption, with values approaching zero signifying increased heterogeneity and a greater deviation from ideal monolayer adsorption.[79] It is important to note that, as an empirical model, the Freundlich equation does not predict a saturation limit; rather, it suggests that adsorption capacity increases indefinitely with increasing equilibrium concentration.

2.2.3.3 Sips

The Sips isotherm model, also referred to as the Langmuir–Freundlich isotherm, is an empirical expression that integrates features of both the Langmuir and Freundlich models to more accurately describe adsorption on heterogeneous surfaces, particularly over a wide concentration range. The model is especially useful for systems where the surface of the adsorbent displays a non-uniform energy distribution yet ultimately approaches saturation at high adsorbate concentrations. As such, the Sips model offers a more generalized and flexible framework for interpreting equilibrium adsorption behavior.

$$q_e = \frac{Q_{mS} K_S C_e^{\beta S}}{1 + K_S C_e^{\beta S}}$$

Equation 18: Sips isotherm modelling equation.

In Equation 18, Q_{ms} (mg/g) and K_s (L m/g) βS are the maximum monolayer saturation capacity and the Sips constant respectively, while β is the heterogeneity factor.[80] Equation 18 reduces to the Langmuir model at sufficiently high adsorbate concentrations, thus predicting maximum surface coverage and reduces to the Freundlich model at low adsorbate concentrations.[79,80] The Sips model behaves similarly to the Freundlich isotherm at low adsorbate concentrations, where the exponential term dominates and multilayer or heterogeneous adsorption is prevalent. At high concentrations, however, the model asymptotically approaches the Langmuir form, thereby predicting a finite saturation capacity and monolayer coverage. This dual behavior enables the Sips equation to overcome the limitations of each individual model, particularly the unbounded adsorption implied by the Freundlich model at high concentrations and the homogeneity assumption of the Langmuir model.[64,79,80]

Due to its versatility and improved fit across both low and high concentration regimes, the Sips isotherm is frequently employed in adsorption studies involving complex adsorbents such as modified activated carbons, polymer-grafted surfaces, and composite materials, where neither Langmuir nor Freundlich alone sufficiently capture the models.

2.2.3.4 Dubinin-Radushkevich (D-R)

The Dubinin–Radushkevich isotherm is a semi-empirical model that provides insight into the energy heterogeneity and mechanistic nature of adsorption processes.

$$q_e = q_m exp^{-\beta(RTln\left(1+\frac{1}{C_e}\right))^2}$$

Equation 19: Dubinin-Radushkevich isotherm.

where q_e represents the amount adsorbed at equilibrium (mg/g), q_m is the theoretical maximum adsorption capacity, and β is a constant related to the mean free energy of adsorption.[69,81] The term $(RTln(1+1/Ce))^2$ corresponds to the Polanyi adsorption potential (ε), which accounts for the work required to move an adsorbate molecule from the bulk solution to the adsorbent surface.[81] Unlike the Langmuir model, which assumes a uniform surface with identical sites, the D-R isotherm accommodates energetic heterogeneity by incorporating a Gaussian distribution of adsorption energies, making it well-suited for materials such as activated carbon-polymer composites that exhibit complex surface characteristics.[82] An important feature of this model is its ability to estimate the mean adsorption energy (E) using the relationship $E = (2\beta)^{-1/2}$, which helps differentiate between physical adsorption (E < 8 kJ/mol) and processes involving stronger interactions such as ion exchange (E = 8.16 kJ/ mol).[83] Because the D-R isotherm integrates both energy distribution and micropore filling

concepts, it is relevant for aqueous systems exhibiting S-shaped isotherms, where cooperative effects, multilayer formation, however the non-uniform energy sites dominating during the adsorption mechanism means that kinetic values received may be less accurate.[65,84]

The D-R isotherm is particularly advantageous for systems with S-shaped isotherms, where cooperative effects and multilayer formation obscure the assumptions of classical models like Langmuir. By emphasizing energy heterogeneity and micropore-filling behavior, the D-R model captures the essential physics of adsorption in environments where multiple mechanisms operate simultaneously. This makes it highly applicable for describing complex, structured surfaces interacting with diverse adsorbates, such as naphthenic acids in oil sands process water, where adsorption cannot be treated as a uniform or isolated phenomenon.

3. Grafting-From Polymerization Via ATRP

3.1 Introduction

Petroleum coke is a carbon-containing solid derived from the refining of crude oil. It is produced during the distillation of crude oil in oil refineries, where high-boiling hydrocarbon fractions, known as "residues," are converted into lighter products such as gasoline and diesel fuel. This byproduct can be used as a precursor to AC, allowing potential remediation of tailing be made of another byproduct of the oil sands industry in Canada.[3,28]

An AC's porous structure can be combined with a tailored surface chemistry enabling it to target specific contaminants. This makes it particularly effective in applications such as water treatment, where it can remove pollutants like organic compounds, heavy metals, and other ions.[85] Additionally, AC can be regenerated and reused multiple times through thermal or chemical processes, reducing waste and lowering operational costs. In environmental remediation efforts, activated carbon plays a crucial role in cleaning up contaminated soil and groundwater by adsorbing pollutants and contaminants, such as petroleum hydrocarbons and volatile organic compounds, thus helping to restore ecosystems and protect human health.

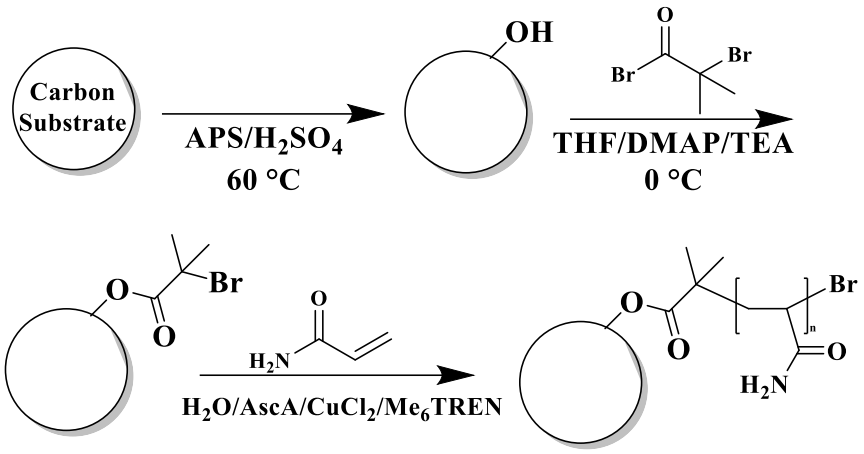

Figure 6: Synthesis scheme for the preparation of petcoke and AC modified substrate for polymerization. Method discussed in section 3.2.2-3.2.5.

AC and petcoke surfaces contain residual heteroatoms (e.g., oxygen, nitrogen) that introduce functional groups capable of influencing hydrophobicity and surface charge.[10,85] These groups Serve as reactive sited for surface-initiated polymerization, making both materials promising substrates for polymer brush formation.[85]

Through covalent grafting, polymer brushes can be grown directly form the surface using ATRP. This approach, grafting-from, allows for dense, uniform polymer coverage, enabling precise control over surface properties. The following sections will explore the comparative suitability of petcoke and AC for grafting-from polymerization and their potential material applications.

3.2 Materials and Methods

3.2.1 Materials

Potassium hydroxide (KOH), ammonium persulfate (APS), and sulfuric acid (H_2SO_4) were purchased from Sigma Aldrich and used as received. Petroleum coke (petcoke) was supplied by Suncor Energy Inc. (Alberta, Canada).

4-dimethylaminopyridine (DMAP), α-bromoisobutyryl bromide (BiBB), tetrahydrofuran (THF), and methanol were purchased from Sigma Aldrich and used as received. Acetone (Fisher Chemicals) were used as received. Triethylamine (TEA) was purchased from thermofisher.

Acrylamide, ethanol, $CuCl_2$, triethylammonium bromide (TEABr), sodium chloride, tris[2-(dimethylamino)ethyl]amine (Me_6TREN), ethyl α-bromoisobutyrate (EBiB), and ethyl 2-chloropropionate (ECP) were purchased from Sigma Aldrich and used as received. CuCl was purchased from Sigma Aldrich and was washed with glacial acetic acid. $CuBr_2$ was purchased from Alfa Aesar and was used as received. N,N,N',N",N"-pentamethyldiethylenetriamine (PMDETA) was purchased from TCI America and was used as received. Ascorbic acid was purchased from Bio Basic and was used as received.

3.2.2 Preparation of AC

Petroleum coke was prepared in accordance with O. Strong et al. (2023). The AC was made using approximately 3.0 g of petcoke and 3.0 g of KOH which were then mixed thoroughly and placed in a stainless-steel crucible. The crucible was placed in an oven under N_2 at 400 °C for 30 minutes and removed once cooled to approximately 200-250 °C. The sample was well mixed and placed back in an oven under N_2 and heated to 900 °C (ramp rate of 60° C/min), then held at 900 °C for 15 min. The sample was allowed to cool to a minimum of 250 °C before removing from the oven. Once cooled to room temperature, the sample was ground with a mortar and pestle, then placed in a beaker with 60 mL of deionized water. The mixture was stirred at 80 °C for 1 h, then vacuum filtered and washed with an additional

60 mL of deionized water at 80 °C. The sample was then stirred with 0.1 M HCl (10 mL /g) at 80 °C for 1 h, then recovered by vacuum filtration. The resulting AC was dried in an oven at 110 °C overnight.

3.2.3 Oxidation

Approximately 1 g of activated carbon was added to a 15 mL solution of 2.0 M ammonium persulfate in 1.0 M sulfuric acid. The mixture was stirred at 60 °C for 1, 4, and 8 h. The mixture was cooled to room temperature and filtered by vacuum filtration. The product was washed with deionized water until the washings were approximately neutral, then dried in a vacuum oven overnight at 110 °C.

3.2.4 Initiator

2.46 g of AC-OH, 0.147 g of DMAP (1.20 mmol), 50 mL of THF, and 2.8 mL of TEA (20 mmol) were added to a 100 mL round-bottom flask. The mixture was dispersed in an ultrasonic bath for 30 min, then transferred to an ice-salt bath and placed under N_2. Once cooled, 1.075 mL of BiBB (8.7 mmol) in 13 mL of THF was added to the flask dropwise. The mixture was stirred on ice for 3 h, then at room temperature for 48 h. The mixture was filtered and washed with acetone, then washed with deionized water. The resulting product was dried in a vacuum oven at 40 °C and denoted as AC-BiBB.

3.2.5 ARGET-Polymerization

0.1035 g of AC-BiBB, 10.662 g of acrylamide (0.150 mols), and 49 mL of Millipore water were added to a round bottom flask and purged with N_2 for 30 min.

0.5 mL of an aqueous catalyst solution containing $CuBr_2$ ($1.5 \cdot 10^{-5}$ mol) and PMDETA ($1.5 \cdot 10^{-4}$ mol) was injected into the flask and sealed under N_2. The solution was heated to 60 °C and 0.5 mL of an aqueous solution containing ascorbic acid ($1.5E10^{-4}$ mol) was injected to initiate polymerization.[36] After 24 h, the solution was cooled and centrifuged at 8700 rpm to collect the product. The supernatant was discarded, and the product was re-dispersed in water and centrifuged again at 8700 rpm. This process was repeated 3 times to remove any free or physically absorbed polymer. The resultant product, denoted as AC-PAM, was collected and dried in a vacuum oven at 40 °C.

3.2.6 Cleavage of PAM

To measure the molecular weight of the grafted polymer, the polymer was first cleaved from the surface of AC by acid-catalyzed hydrolysis. This was accomplished by refluxing 0.5 g of AC-PAM with 25 mL of Millipore water and 0.25 mL of concentrated HCl at 100 °C for 3 hours. After the reflux was complete, the solution was cooled to room temperature and vacuum filtered to remove the AC. The filtrate was precipitated in excess methanol and vacuum filtered to recover the cleaved polymer. The cleaved polymer was dried in an oven at 40 °C overnight.

3.2.7 Characterization

The elemental composition of the activated carbon and oxidized activated carbon samples were measured by XPS. XPS measurements were performed on a Kratos AXIS supra spectrometer using monochromatic Al K(alpha) source (15 mA, 15 kV). The instrument work function was calibrated to give a binding energy (BE) of 83.96 eV for the Au 4f 7/2 line for metallic gold, and the spectrometer dispersion was

adjusted to give a BE of 932.6 eV for the Cu 2p3 eV line of metallic copper. The Kratos charge neutralizer system was used on all samples. Survey scan analyses were carried out with an analysis area of 300 · 700 microns and a pass energy of 160 eV. High resolution analyses were carried out with an analysis of 300 · 700 microns and a pass energy of 20 eV. Analysis of the survey scans and high-resolution scans were performed using CASA XPS, with spectra being corrected to the main line of the C1s spectrum at 284.8 eV. Baseline corrections were made using a Shirley type background correction.

The molecular weight and molecular weight distribution of the cleaved polymer was determined by size exclusion chromatography (SEC) using Agilent Technologies 1220 Infinity LC equipped with a refractive index detector (RID, Agilent Technologies 1260 Infinity). Please refer to section 2.1.1 Size Exclusion Chromatography (SEC) for more information.

3.3 Results and Discussion

3.3.1 Comparison of Petcoke and AC as a Substrate

To better understand the importance of the substrate in the performance of the grafting-from polymer approach, petcoke was evaluated alongside AC. Both materials serve as carbon-rich base, but petcoke offers potential advantages, including cost-effectiveness and abundant availability. Importantly, this investigation aimed to determine whether petcoke could serve as a viable alternative substrate for the surface-initiated polymerization of polyacrylamide.

The goal was to observe whether petcoke could be an equivalent or better substrate than compared to the AC substrate. To attach the initiator, the substrate must

first be oxidized to add hydroxy functionality. Below is a summary of the attempts made and a comparison to the AC-OH.

Table 2: Oxidized Petcoke vs Oxidized AC.

Sample Name	Elemental Compositions			
	C	O	N	S
Ground Petcoke 75% micron (Reference Sample, not oxidized)	85.1±4.2	6.8±0.9	1.3±0.2	2.1±0.8
Untreated Petcoke	74.5±3.2	14.7±0.8	1.2±0.2	2.2±1.7
Heat-Treated Petcoke	83.3±1.7	17.6±3.0	1.3±0.5	1.6±0.7
Activated Carbon Average	79.1±1.0	16.72±1.2	1.7±0.3	-

Table 2 summarizes the elemental composition of oxidized untreated and heat-treated petcoke samples in comparison with oxidized AC. As expected, oxidation increased the oxygen content across substrate samples, albeit with some minor variability. Notably, the heat-treated petcoke samples demonstrated a higher carbon to oxygen ratio than untreated samples, which may suggest a more selective oxidation or thermal stability of certain surface groups.[86,87] The AC displayed a relatively balanced C:O ratio, which are comparable to that of the functionalized petcoke. One of the challenges observed was the elevated sulfur content in petcoke, particularly in untreated samples. This is of concern because sulfur species can interfere with radical polymerization mechanisms and may require extensive washing to remove.[88–90] Although the application of concentrated acid treatments did lower the sulfur levels, such aggressive conditions risk degrading surface features critical for grafting. As a future direction, optimizing the oxidation process to balance sufficient oxygen

functionalization with minimal surface damage, and reduced sulfur contamination may enhance petcoke's usability.

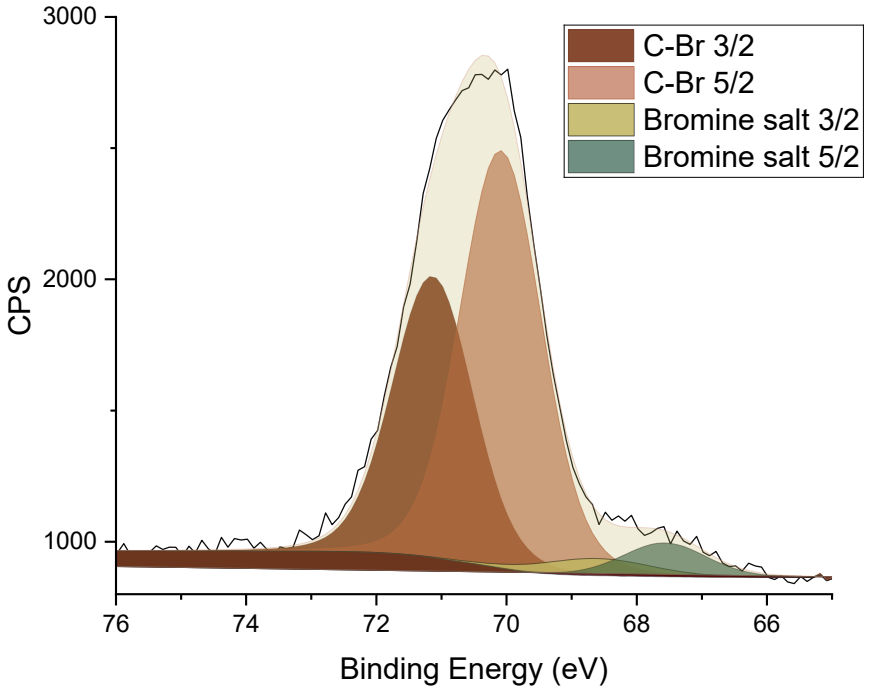

Figure 7: XPS of initiator attachment (BiBB) for petroleum coke.

Following surface oxidation, the ATRP initiator, α-bromoisobutyryl bromide (BiBB), was introduced to both petcoke and AC substrates. Table 3 presents the elemental analysis post-initiator attachment, with particular attention to bromine content as a marker of successful introduction of the initiator.

Table 3: Initiator attachment to petcoke vs AC.

Sample Name	Elemental Compositions				
	C	O	N	Br	S
Untreated Petcoke	85.1±4.2	6.8±0.9	1.3±0.2	2.1±0.8	85.1±4.2
Heat-Treated Petcoke	74.5±3.2	14.7±0.8	1.2±0.2	2.2±1.7	74.5±3.2
Activated Carbon Average	83.3±1.7	17.6±3.0	1.3±0.5	1.6±0.7	83.3±1.7

Petcoke samples consistently demonstrated Br concentrations near or above 0.9 at%, slightly higher and more uniform than the Br content observed on AC (~0.6 at%). This suggests that petcoke, particularly after proper surface treatment, may even offer more consistent initiator coverage than AC, which could contribute to better control over polymer brush growth.

3.3.2 Successful Grafted Polymer

3.3.2.1 Polymerization and HPLC Analysis

Once the initiator was successfully attached to multiple substrates, surface-initiated polymerization of acrylamide was conducted using ATRP method under ambient conditions. The goal was to evaluate polymer brush formation and molecular characteristics such as M_W, with a goal of 1,000,000 g/mol. Dispersion of a value under 1.5 for controlled polymerization, and monomer conversion rates.

Table 4 compares PAM grafting results between petcoke and AC substrates. Interestingly, untreated petcoke sample C achieved the highest monomer conversion (63 %) and Mn (346,089 g/mol), though it also had the broadest Đ (2.27). This suggests rapid growth and chain termination events, likely due to the heterogeneous nature of the untreated surface. Heat-treated petcoke (sample A) exhibited a slightly

lower conversion (58 %) and M_n (195,431 g/mol) but a narrower Đ (1.95), indicating more controlled polymer growth. In comparison, the AC-grafted PAM sample polymerized under the same conditions showed a conversion of 62 % and M_n of 263,738 g/mol with a Đ of 2.20. These findings demonstrate that petcoke can support polymer brush growth comparable to, and in some cases exceeding, that of AC. The broader molecular weight distribution on petcoke suggests further optimization is needed, but its potential as a functional grafting platform is evident.

Table 4: Grafting-from approach comparing petcoke vs AC substrate.

Sample Name*	Temperature	Monomer Conversion (%)	Mn (g/mol)	Đ
Untreated petcoke	r.t	63	745,000	2.27
Heat-treated petcoke	r.t	58	395,000	1.95
Activated Carbon	r.t	62	664,000	2.20

*15000:1:0.5:1:1 in 50 mL solution

3.3.2.2 Covalently Bound Polyacrylamide

To verify that the PAM chains were covalently grafted onto the AC surface rather than merely physiosorbed, thermogravimetric analysis (TGA) was performed on both the initiator-modified AC and the final composite materials. TGA was used to estimate the amount of PAM grafted from the AC surface by measuring the residual weight at 1,000 °C. The increase in residual mass of the AC-PAM composites, relative to pure PAM, was attributed to the inorganic content of AC (Table 5). A shift in residual weight and temperature between a grafted and un-grafted AC-PAM could indicate whether the polymer was covalently bound to the surface. When the grafted

polymer was compared to the free polymer, there was an increased temperature prior to the initial mass loss.

Table 5: Residual weight % at 1,000 ºC of SI-ATRP PAM with different substrates.

Polymer Substrate	Residual wt % at 1,000 ºC	Carbon Substrate content (wt %)
Untreated petcoke	11.0 ± 0.1	4.3 ± 0.2
Heat-treated petcoke	8.9 ± 0.2	0.4 ± 0.2
Activated Carbon	15.8 ± 0.6	6.1 ± 0.4

The calculated AC content in each AC-PAM sample depended on both the amount of AC initiator used in the polymerization reaction (reflecting the degree of polymerization) DP and the total mass recovered after polymerization. For example, the sample heat-treated petcoke, exhibited the lowest carbon content (0.4 wt%) due to its high polymer yield (90%), resulting from a higher DP of approximately ~5,000. In contrast, the activated carbon sample showed significantly higher substrate contents of 6 %, respectively. These samples had both a lower DP (1,000) and lower mass yields (60 %), which increased the relative proportion of AC in the final composite. These results demonstrate that surface-initiated ATRP is capable of producing dense, high molecular weight PAM brushes even when the starting AC content is minimal. This high efficiency in grafting supports the effectiveness of the SI-ATRP method for tailoring polymer–substrate interfaces with well-controlled architecture and composition. Furthermore, there is a shift in degradation of the carbon substrate between grated and un-grafted PAM indicating the polymer is covalently attached to the surface of the activated carbon. This is seen with an initial degradation of 800 °C to 500 °C of the polymers.

The grafting can also be characterized through imaging. It is particularly useful for imaging interfaces within polymer matrices, identifying particle distribution, and performing elemental analysis through techniques such as TEM and STEM. These methods allow for more detailed information on the structure of the polymer composites and can specifically identify different elemental compositions and different points.

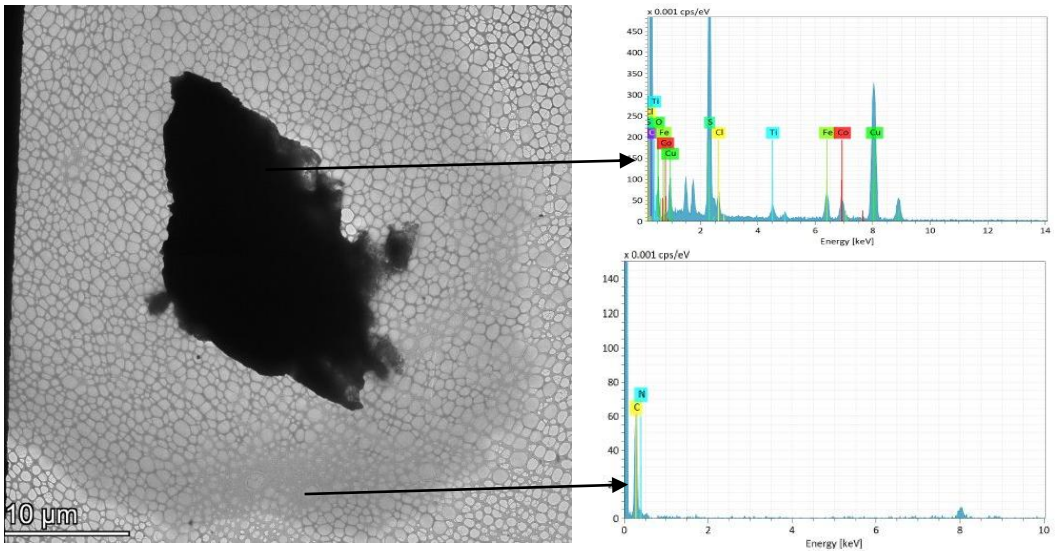

Figure 8: STEM & TEM imaging of Cu (0) mediated polymerization “grafted from” activated carbon.

As shown in Figure 8, the halo surrounding the black particulate in the center retains only carbon and nitrogen, with an approximate 3:1 ratio based on the peak area. This indicates that the halo is made up of polyacrylamide. The center portion displaces numerous compounds, which is expected with the activated carbon process, specifically the high carbon and sulphur content, in addition to the presence of copper, which comes from the catalyst during polymerization. Note the AC particles were sized prior to polymerization to help identify them during imaging.

3.3.3 Variation on Polymerization

Following the successful grafting to both petcoke and AC via surface-initiated polymerization, further efforts were made to improve both the polymer yield and molecular weight (M_W) of grafted PAM. Several modifications to the ATRP procedure were explored, including the late-stage addition of reaction components along with variation to the ATRP mechanism as discussed in Table 1. Optimizing M_W is critical for flocculation performance, as longer polymer chains enhance bridging between particles, while higher yield reflects the completeness of polymerization and the degree of control over the reaction.

The first strategy tested was the delayed addition of copper metal. However, this approach was unsuccessful, resulting in a monomer conversion of less than 10%. This poor outcome is attributed to the premature formation of radicals due to the early presence of ascorbic acid (AscA), the ligand, and the initiator. Without sufficient copper present to mediate the reaction from the beginning, radical termination occurred rapidly, hindering polymer chain propagation. Next the late addition of the reducing agent was tested. Ascorbic acid was added at 0.2 mol equivalence and resulted in much higher yields, indicating efficient monomer conversion. However, despite improved conversion, there was no significant increase in the molecular weight of the resulting PAM. These results suggest that while delayed reducing agent addition can drive conversion, it does not alone enhance control over polymer chain growth or dispersity.

The most promising approach involved the delayed or gradual addition of ligands, which was investigated both as a periodic addition over time and as a single delayed dose. Table 6 summarizes the resulting polymer properties from these trials.

Table 6: Late addition polymerization.

Sample Name*	Additional AscA (mg)	Late L Addition (min)	Monomer Conversion	Mn (g/mol)	Đ
AC-PAM A	10	300	94	120, 000	1.35
AC-PAM B	-	10	89	1,150,000	1.29
AC-PAM C	10	10	91	1,000,000	1.41
AC-PAM D	50	10	86	2,000,000	1.38
AC-PAM E	-	50	79	95,000	1.45

*500:1:0.5:1:1:1 in 50 mL

In Sample C, ligand was gradually introduced over a 12 h period, resulting in a high yield (90 %) and a significant increase in M_n (>1.15 kg/mol), with a relatively low dispersity (D = 1.32). In Sample D, the same periodic ligand addition was paired with a late addition of AscA. This combination reduced the yield slightly to 80% but resulted in a modest further increase in M_n (~1.23 kg/mol). Samples E through H were modified by delaying all ligand addition until 2 h into the reaction, allowing copper (II) to slowly reduce to copper (I) in the absence of ligand coordination. These samples produced substantially higher molecular weights, with Sample G reaching an M_n of over 2.25 kg/mol. Although yields did not exceed those from standard conditions, they remained robust (80%), indicating the technique's effectiveness in promoting chain growth without compromising conversion. These experiments demonstrate that ligand coordination timing is a critical variable for controlling polymer architecture in SI-ATRP and can significantly influence the final M_W without severely compromising monomer conversion.

Both petcoke and AC substrates functionalized with surface-bound initiators were tested under identical “grafting-from” polymerization conditions to assess performance differences. As shown in Table 4, both substrates supported successful

PAM growth via ATRP, yielding comparable molecular weights (Mn = 745,000 for petcoke vs. 664,000 for AC) and moderate dispersity's (Đ = 2.27 and 2.20, respectively). This supports earlier findings that petcoke is a viable alternative to AC for surface-initiated polymer brush synthesis.

Dispersity values for both substrates remained relatively high, indicating that while polymerization was successful, control over chain length uniformity could be improved further. This aligns with earlier observations from the optimization section, where strategies like delayed ligand addition led to better control and narrower Đ. Both substrates with initiator functionalized to the substrate were used during grafting-from polymerization. As can be seen in Table 4 and Table 7, both the petcoke and AC functioned as a substrate for various ATRP polymerization and resulted in similar molecular weights. It should be noted that both methods using the ATRP resulted in broad dispersity.

Table 7: Polymerization of different ATRP method with P-BiBB.

Sample Name	Monomer Conversion (%)	Mn (g/mol)	Đ
Free ATRP	63	346,000	2.27
ARGET	81	1,700,000	1.23
ATRP	70	2,500,000	1.38
SET-LRP	0	-	-
SARA	63	5,200,000	1.25

Polymerizations were also conducted using P-BiBB, a petcoke-based initiator functionalized similarly to AC-BiBB. These experiments (Table 7) were performed under varying conditions using copper in different oxidation states (Cu (0), Cu (I), Cu (II)). Although results are not directly comparable to earlier surface

polymerizations due to differences in concentration and setup, the findings are still significant. The Cu (II) system produced the highest monomer conversion (80 %) and a very high molecular weight (Mn = 1.72 kg/mol) with excellent control (Đ = 1.23). The Cu (I) system also achieved high molecular weights, though full data were not recorded. The Cu (0) system, however, failed to initiate polymerization, yielding no product. This may suggest that P-BiBB is less effective at coordinating or reducing Cu (0), or that the system kinetics were not favorable under the given conditions. These data confirm that P-BiBB behaves similarly to AC-BiBB as a surface-bound initiator, especially in copper-mediated ATRP systems involving Cu (I) and Cu (II), making it a suitable substrate for advanced polymer brush applications.

Overall, the petcoke is a suitable substrate for various ATRP methods. Although the initial washing of the AC-OH is much longer it results in greater hydrophobicity than AC and thus may be more effective during flocculation. The polymerization itself has the same duration as petcoke when compared to the AC, however, the overall conversion was improved with both the Cu (I) and Cu (II) systems. Current P-BiBB samples do not allow for polymerization with Cu (0).

3.3.4 Flocculation

While the central focus of this thesis is on the adsorption behavior and surface interactions of polymer-grafted carbon materials, it is essential to demonstrate that their primary intended function, flocculation, can also be effectively achieved. Flocculation is a critical process in oil sands tailings treatment, see Section 1.1 Flocculation of Mature Fine Tailings. Therefore, a more in-depth analysis of adsorption behavior is beyond the scope of this chapter, a comparative evaluation of

flocculation performance was conducted to validate the materials' applicability for tailings management.

Table 8 presents a summary of flocculation performance metrics obtained from batch experiments using 5 wt% MFT. Several polymer-functionalized petcoke composites synthesized via different ATRP techniques were evaluated alongside an industry-standard flocculant. The performance was assessed by measuring initial settling rate, capillary suction time (CST), supernatant turbidity, and final solids content after dewatering.

Table 8: Comparative flocculation of alternative substrates and polymerization.

Sample Name	Dosage (ppm)	Initial Settling Rate (m/hr)	Capillary Suction Time (s)	Supernatant Turbidity (NTU)	Solid Content (%)
Free Polymer	10,000	13	10	3	21
Petcoke-ATRP	10,000	8	20	40	9
SI-ATRP	8,000	2	5	10	4
ARGET -ATRP	8,000	5	10	10	3
SARA-ATRP	5,000	2	5	5	21

Among the tested materials, SARA-ATRP-modified petcoke exhibited the most promising flocculation behavior. At a relatively low dosage of 5,000 ppm, it produced dense flocs with a rapid initial settling rate, short CST (5 s), low residual turbidity (5 NTU), and a final solid content of 2 %, which significantly outperforms the industry standard in water release. These values suggest that the SARA-based polymer system is highly effective at promoting both particle aggregation and water release, likely due to optimized polymer graft density and chain mobility that favor bridging interactions. By contrast, the SI-ATRP and ARGET-ATRP systems required

higher dosages (8,000 ppm) and yielded lower settling rates and solid content, indicating less efficient bridging or possibly suboptimal surface coverage. While both systems improved turbidity and CST relative to baseline, their performance metrics suggest that either steric hindrance or insufficient chain extension may have limited their effectiveness. Petcoke-ATRP sample, lacking surface-initiated control, showed higher turbidity and CST, likely due to irregular polymer architecture and a more heterogeneous surface, which may have contributed to floc instability and poor water release.

These preliminary flocculation results demonstrate that controlled polymer grafting can significantly impact the performance of carbon-based flocculants. SARA-ATRP shows considerable promise for improving both floc structure and dewatering performance at lower dosages. While detailed dosing ranges or sedimentation modeling are not included here, these results establish a strong foundation for future optimization of polymer architecture and surface functionality to target flocculation specifically. For the purposes of this thesis, however, these findings serve to confirm that the developed materials are functionally competent as flocculants, enabling the shift of focus in subsequent chapters to their adsorption behavior.

3.4 Conclusions

In conclusion, this study demonstrates the viability of petcoke as an alternative carbon substrate for surface-initiated polymerization using the ARGET-ATRP method. Through systematic comparison with AC, petcoke was shown to support comparable levels of surface oxidation, initiator attachment, and polymer grafting efficiency. While variability in elemental composition, particularly sulfur content, poses

challenges, optimized oxidation and surface treatment methods mitigated many of these limitations. Notably, petcoke samples achieved high monomer conversions and molecular weights, suggesting strong potential for controlled polymer growth. These findings highlight petcoke's promise as a low-cost, abundant, and functional substrate for advanced polymer composite applications, laying the groundwork for further exploration into sustainable materials engineering.

4. Adsorption Study

4.1 Introduction

Adsorption is a widely used technique for removing organic contaminants from aqueous environments, with AC being one of the more effective adsorbents due to its high surface area, porous structure, and various low-cost feedstocks.[11] These features make it particularly appealing for treating complex industrial waste waters such as oil sands process-affected water (OSPW). Activated carbon has demonstrated high adsorption capacities, up to 400 mg/g for some model naphthenic acid species.[29] This material can be scaled up for water treatment application.

The composite material examined in Chapter 3 incorporates approximately 5 % activated carbon relative to the polymer grafted onto its surface. While the primary role of this composite is in flocculation, its adsorption capabilities remain underexplored, specifically related to structurally diverse contaminants like naphthenic acids in OSPW. To better understand these interactions, adsorption studies must examine performance as a function of specific molecular structures and physicochemical properties.

Equilibrium adsorption data, modeled through isotherms such as Langmuir, Freundlich, Sips, and D-R are critical for evaluating adsorbent performance. These models help characterize adsorption capacity, surface heterogeneity, and binding affinity, and provide a basis for optimizing the composite materials.[68] Polymeric materials, in particular, offer the advantage of tunable chemical composition and surface functionality, enabling selective adsorption when designed appropriately.

While adsorption plays a vital role in contaminant removal, the broader challenge of tailings management in Alberta’s oil sands also hinges on effective

dewatering. The oil extraction process generates vast volumes of tailings containing sand, clay, and residual bitumen, which are stored in tailings ponds. Over time, fine particles form a stable suspension known as mature fine tailings (MFT), which resist natural settling due to electrostatic repulsion. With current dewatering technologies recovering only about 70 % of water, significant advances are needed to meet regulatory requirements for land reclamation.[91] These water-soluble polymers function through mechanisms including depletion, charge patch, and bridging flocculation, each dependent on polymer charge and molecular weight.

To enhance performance, PAM is frequently copolymerized with ionic or hydrophobic monomers. Cationic variants can improve particle adhesion but risk collapsing onto surfaces, reducing bridging efficiency. Anionic PAMs, particularly those with optimal charge density and high molecular weights, offer better bridging behavior but suffer from high hydrophilicity, which hinders dewatering performance. As a result, recent research has focused on introducing hydrophobic monomers—such as t-BAAM and NIPAM-into PAM chains to improve water release and flocculation efficiency in MFT treatment. This work aims to integrate insights from adsorption to help support flocculation science to evaluate how composite materials incorporating activated carbon and functionalized polymers interact with diverse organic contaminants in OSPW, offering a potential dual-function approach for enhanced tailings remediation.

4.2 Materials and Methods

4.2.1 Materials

Diphenylacetic acid (DPA), succinic acid (SA), benzoic acid (BA), and sodium dodecyl-d_{25} sulfate were all purchased from Sigma Aldrich. Buffer solution was made using sodium phosphate dibasic obtained from bioshop and sodium phosphate monobasic obtained from westlab.

4.2.2 Batch Adsorption Method

All adsorption experiments presented here followed the procedure provided in Chapter 2 Section 2.3.1.

4.3. Results and Discussion

4.3.1 Batch Adsorption

Batch adsorption is a widely used experimental approach to evaluate the capacity and efficiency of adsorbent materials in removing target contaminants from solution under controlled conditions. In this method a fixed amount of adsorbent is mixed with a known concentration of adsorbate, and the reduction in concentration is monitored over time to determine adsorption performance.[75] It is particularly useful for screening adsorbent materials and understanding the influence of surface chemistry, functionalization, and material dosage on adsorption behavior.[74] In this study, batch adsorption experiments were conducted to obtain kinetics and isotherm data for benzoic acid to compare the performance of substrates modified by different ATRP techniques. There are numerous model NAs that could be investigated for uptake onto AC substrates with graphed polymers, however, in previous work benzoic acid (BA) displayed a moderately good affinity for AC and a good affinity with AC-

PAM and thus will primarily be studied as the most replicable compound. Later in this chapter adsorbates with slower/lower uptake will be discussed in terms of isotherms.

The adsorption behavior of benzoic acid across variously modified substrates reveals insights into how surface grafting via different ATRP techniques influences functional performance. Figure 9 shows that the un-grafted substrate (AC-BiBB) exhibits minimal adsorption, with values ranging only from ~10-20 % even as the dosage increases from 50 mg to 150 mg in 50 mL. This suggests that the inherent surface chemistry of the substrate lacks the necessary functional groups or accessible sites required for effective benzoic acid interaction, which is further confirmed by the loss of surface area from ~1000 m^2/g to 50 m^2/g determined using BET. In contrast, all three composite materials with grafted polymer observed increased uptake of BA. Given that on average only 5 % of the composite material is made up of the modified AC, the enhanced uptake observed in the modified samples must be due to the presence of surface-grafted polymers. As polyacrylamide contains amide functionalities capable of engaging in hydrogen bonding and dipole–dipole interactions with benzoic acid (a weak aromatic acid), these groups likely serve as the primary adsorption sites.

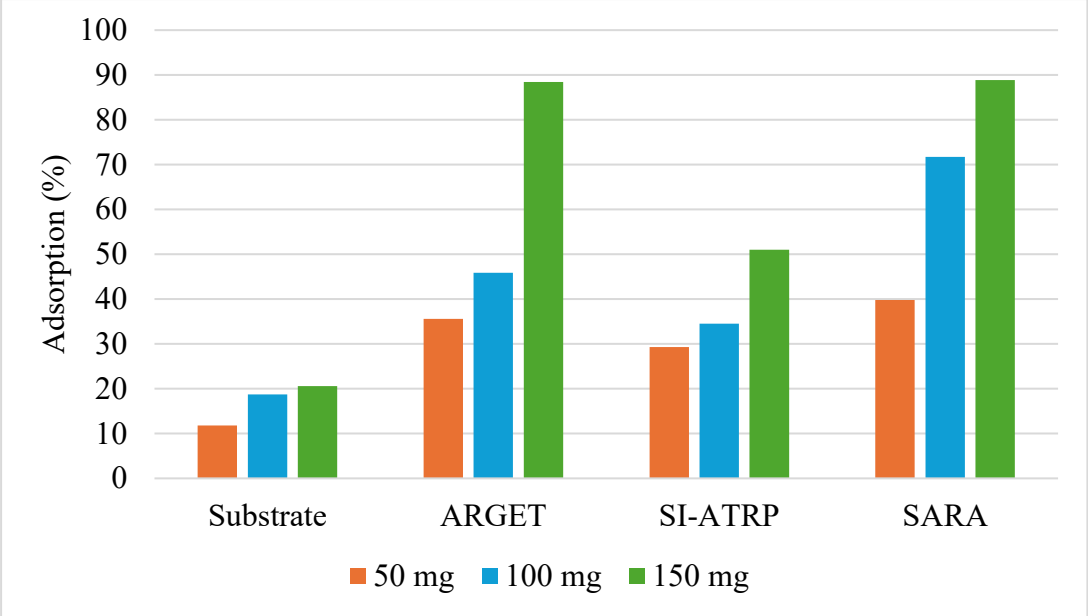

Figure 9: Comparison of adsorption data for successful AC grafted polymers shown in Table 7. All tests were performed with 60 ppm stock solution of benzoic acid.

Among the modified samples, ARGET and SARA ATRP methods result in higher adsorption efficiencies compared to SI-ATRP. At the highest dose (150 mg), both ARGET and SARA achieve adsorption levels near or above 90 %, while SI-ATRP only reaches about 50 %. This discrepancy aligns well with the polymerization characteristics reported in Table 7. ARGET and SARA not only exhibit higher monomer conversions (81 % and 63 %, respectively) but also yield polymers with high molecular weights ($M_n = 1.7 \times 10^6$ g/mol for ARGET and 5.2×10^6 g/mol for SARA) and narrow dispersity ($Đ \approx 1.23$ - 1.25). In contrast, SI-ATRP results in a lower molecular weight ($M_n = 3.46 \times 10^5$ g/mol) and a broad dispersity ($Đ = 2.27$), indicative of poorer control over the polymerization process. These differences in polymer characteristics directly impact how the chains arrange themselves on the substrate surface, which, in turn, governs the accessibility of adsorption sites.

In well-controlled polymerization, the resulting polymer brushes are typically more uniform in length and exhibit a dense, extended conformation perpendicular to the surface.[38,92,93] This "brush" architecture minimizes entanglement and maximizes the exposure of amide groups along the polymer backbone, enhancing their availability for interactions with adsorbate molecules. In contrast, a polymer that is shorter and polydisperse, can lead to a more disordered or "mushroom-like" configuration that may collapse back onto the substrate surface.[30,37,94,95] In such a conformation, many adsorbent sites may become sterically hindered or buried within the polymer matrix, thereby reducing their effective accessibility for adsorption. The nature of controlled polymerization allows for low dispersity, under 1.5 Đ, which indicates good uniformity regardless of molecular weight. However longer and more densely packed polymer can lead to entanglement and gelling, whereas the lower molecular weight and low-density polymers may result in looping, or “mushroom” shaped surfaces.

The differences in polymerization mechanisms between ATRP methods provide further insight. ARGET employs a reducing agent to continuously regenerate the active Cu (I) species, allowing sustained polymer chain growth with minimal catalyst concentration. This not only limits metal contamination but also supports more uniform and prolonged polymer growth. SARA, which relies on Cu (0) and supplemental Cu (II), also enables a high degree of control, with disproportionation and regeneration cycles favouring uniform chain propagation. In contrast, SI-ATRP often involves immobilized initiators on the surface and lacks the dynamic activator/deactivator equilibrium found in ARGET and SARA, leading to less controlled polymer structures and reduced functional group exposure.

Overall, the superior adsorption observed with ARGET and SARA ATRP is a consequence of both higher polymer quality, characterized by increased molecular weight and narrower dispersity, and favourable chain orientation that maximizes exposure of amide groups (Table 7). This section indicates that the polymer's morphology will have an impact on the uptake of the adsorbate.

4.3.2 Kinetics

Three NAs were studied with differing structures. Diphenyl acetic acid (DPA), benzoic acid (BA), and succinic acid (SA), display different levels of hydrophobicity, to help understand the multitudes of variability in NAs in OSPW. The kinetic adsorption displays minor differences in the interaction between the polymer composite and each of the three naphthenic acids over a 360-hour period. All three acids show time-dependent adsorption behavior, indicating a gradual diffusion-controlled process, as the mixing speed for these tests was 250 rpm which should make external diffusion time negligible. Among the acids, succinic acid (SA) demonstrates the highest adsorption capacity, reaching nearly 65 % adsorption by the end of the experiment. In contrast, benzoic acid (BA) reaches a plateau around 45 %, while diphenyl acetic acid (DPA) shows the lowest adsorption performance, not exceeding 38 % throughout the duration.

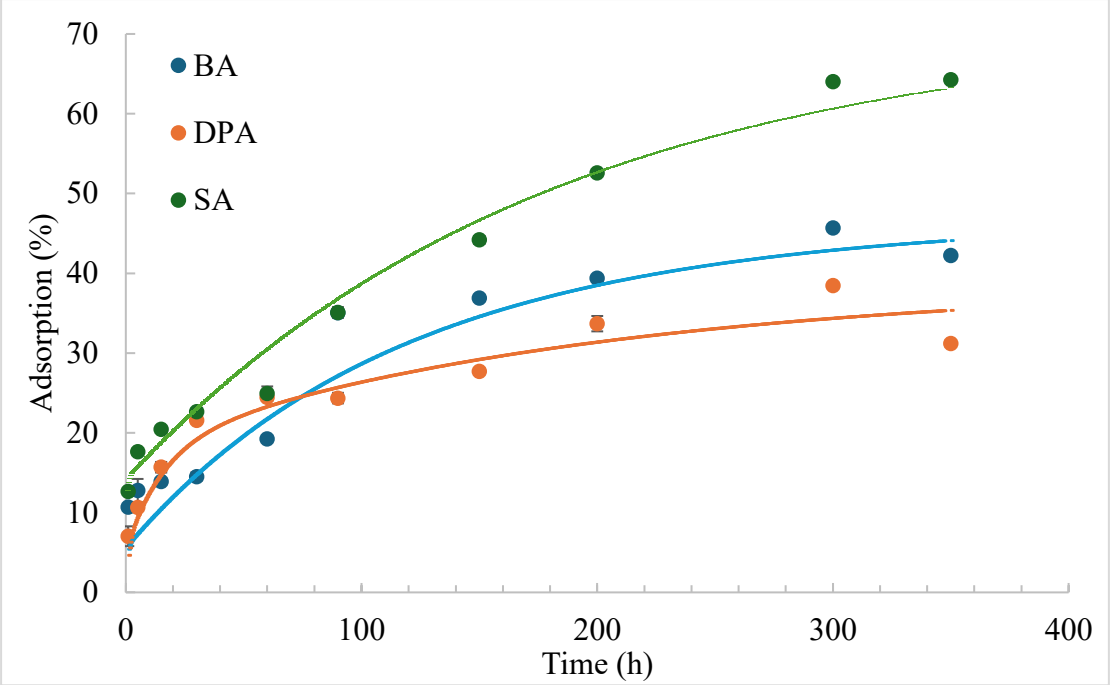

Figure 10: Kinetic of three model naphthenic acids, benzoic acid (BA), phenylacetic acid (DPA), and succinic acid (SA). SARA-ATRP composite material, modelled using m-exp.

These differences are likely attributed to the molecular structure, pKa, polarity, and size of the naphthenic acids. SA is a relatively small, aliphatic diacid, although it is hydrophilic and will not readily interact with the AC substrate it may have more affinity for the available amide groups in polyacrylamide.[96] Its higher hydrophilicity may also facilitate better interfacial compatibility with the polar surface of the polymer composite. In contrast, DPA, with its bulky aromatic structure and two phenyl rings, may experience steric hindrance and reduced accessibility to internal adsorption sites. Additionally, the aromatic ring systems in DPA and BA may engage in π–π stacking or hydrophobic interactions; however, these are typically weaker and more geometrically constrained than the hydrogen bonding or electrostatic attractions favored by SA.[59,97] Due to the rigid, planar nature of aromatic systems, such interactions require specific alignment and proximity, which may be hindered by steric bulk or unfavorable orientation within the polymer matrix. In contrast, SA's

small, flexible structure and high polarity allow it to more readily access and interact with amide groups and polar domains within the composite.

The kinetic trends suggest distinct adsorption mechanisms for each naphthenic acid, as reflected in both the uptake profiles and estimated half-lives. SA exhibits the longest half-life at 83.80 hours, consistent with its delayed yet sustained adsorption, likely a result of its strong polarity and compact size, which promote gradual infiltration into the brush layer. In contrast, DPA, with a half-life of 30.69 hours, demonstrates more rapid initial adsorption that plateaus quickly, potentially due to steric hindrance from its bulky aromatic structure that limits deeper diffusion. BA falls between the two, with a half-life of 68.08 hours, suggesting moderate interaction driven by its single aromatic ring and intermediate size. The extended timescale for maximum adsorption (exceeding 300 hours) underscores the role of the polymer matrix in regulating solute transport, likely through a combination of crosslinking and brush density that restrict diffusion.

4.3.3 Isotherms

To evaluate the adsorption behavior of AC-PAM composites synthesized via ARGET, SARA, and conventional ATRP, equilibrium isotherm modeling was performed using benzoic acid (BA), diphenyl acetic acid (DPA), and succinic acid (SA) as model NAs. These analytes were selected to probe the influence of both steric bulk and hydrophobicity, with BA serving as a monoaromatic control, DPA representing a bulkier hydrophobic molecule, and SA embodying a small, polar dicarboxylic acid. This molecular diversity provides mechanistic insight into how polymer brush architecture, crosslink density, and surface heterogeneity effect adsorbate uptake.

The isotherm models evaluated include Langmuir, Freundlich, Sips, and Dubinin-Radushkevich (D-R), each reflecting a distinct assumption about the surface chemistry and absorption mechanisms. Langmuir modeling enables quantification of theoretical monolayer coverage and surface saturation, assuming uniform site energy and no solute-solute interactions.[77] Freundlich fitting, by contrast, accommodates energy heterogeneity and multilayer development but lacks a defined saturation point, rendering its parameters semi-empirical and more indicative of surface affinity than absolute capacity.[79] The Sips hybrid model accounts for both Langmuir-type saturation and Freundlich-like site diversity and was particularly useful in characterizing mildly sigmoidal uptake curves observed in ARGET-functionalized systems (Table 11).[80] The D-R model, underpinned by Polanyi's potential theory, which offers a thermodynamically grounded approach for systems dominated by micropore volume-filling, rather than classical surface adsorption, this yields energetic parameters that approximate the mean free energy of sorption.[69,81] However, this model also introduces key limitations, particularly in aqueous systems where hydrogen bonding, desolvation, and chemisorptive effects confound purely physical uptake mechanisms.[98]

Table 9: Modelling evaluation for the best fitted isotherm models used for each adsorption system.

Model NA	Adsorbent	Best Model	X^2	Adj R^2	AIC_c
BA	ATRP	Sips	4.17	0.903	6.42
	ARGET-ATRP	D-R	2.02	0.980	4.88
	SARA-ATRP	D-R	0.633	0.855	1.69
DPA	ATRP	D-R	0.121	0.850	1.51
	ARGET-ATRP	D-R	0.9776	0.98966	18.616
	SARA-ATRP	D-R	1.06007	0.49119	2.514
SA	ATRP	-	-	-	-
	ARGET-ATRP	Langmuir	0.00184	0.959	7.997
	SARA-ATRP	D-R	0.37922	0.67394	8.350

Table 9 presents a comparative evaluation of isotherm model fitting across different adsorption systems. For benzoic acid (BA) adsorbed onto ATRP surfaces, the Sips model was identified as the best fit, with adjusted R^2 of 0.903 and a corresponding AICc of 6.42. Although the Langmuir model produced a similar R^2, the Sips model was favoured due to its lower AICc, which penalizes for model complexity and better reflects overall explanatory power. This suggests that BA adsorption may involve cooperative interactions or heterogeneous binding sites, consistent with the mildly sigmoidal uptake behaviour observed. For ARGET-ATRP surfaces, BA adsorption was best described by the D-R model, which yielded an adjusted R^2 of 0.980 and an AICc of 4.88. The strong fit and low AICc support the interpretation that micropore filling or energetically distributed binding sites may dominate in this system. Similarly, the SARA-ATRP composite showed best fit with the D-R model (Adj $R^2 = 0.855$, AICc = 1.69), reinforcing the relevance of pore-filling mechanisms for BA across controlled polymerization methods.

The consistently low AICc values observed for the D-R model across multiple systems reflect its strength in capturing adsorption behaviour where micropore filling, rather than surface saturation, dominates. Unlike Langmuir or Sips models, which assume discrete site occupancy, the D-R model accommodates a continuous energy distribution and volume-based sorption, making it particularly well-suited for systems involving complex polymer architectures and sterically hindered analytes.

4.3.3.1 Conventional ATRP Composites

Polymer brushes synthesized via conventional ATRP showed moderate molecular weights (Mn ≈ 2.5 kg/mol) and broader dispersity (Đ ≈ 1.38), suggesting reduced control over polymer architecture This likely contributes to surface

heterogeneity and inconsistent binding behaviour across adsorption sites. Adsorption of benzoic acid (BA) was best described by the Sips model, which yielded an adjusted R^2 of 0.903 and an AICc of 6.421 (Table 9). While the Langmuir model produced a similar adjusted R^2 (0.903), its AICc was slightly higher, suggesting that Sips offers a marginally better balance between fit quality and model complexity. The use of comparative AIC values indicate that it is not the complexity of the Sips model that allows for a better fit but the values themselves. This is indicated by the n value being <1. The Freundlich model, though often used to describe heterogeneous surfaces, returned a higher AICc and less favorable parameter stability. The D-R model performed poorly (Adj R^2 = 0.674), and its fit was not supported by the data. These results suggest that BA adsorption on conventional ATRP composites may involve cooperative interactions or site diversity, consistent with the mildly sigmoidal uptake behavior captured by the Sips model.

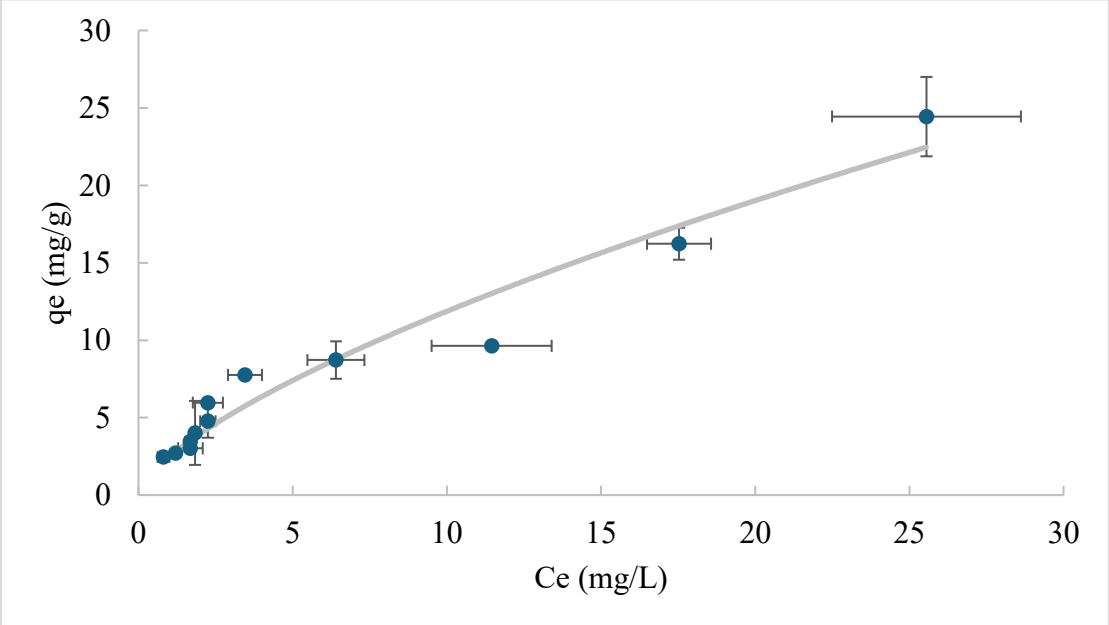

Figure 11: Isotherm for BA on conventional ATRP composites. Modelled using Sips.

For DPA only the D-R model provided a viable fit, with an adjusted R^2 of 0.850 and an AICc of 1.51. Langmuir, Freundlich, and Sips models returned unstable or non-physical parameters, including negative values and poor convergence. The D-R model's ability to accommodate Gaussian energy distributions and volume-filling behavior makes it particularly suitable for describing adsorption of bulkier, hydrophobic molecules like DPA. However, despite the relative fit, the model exhibited high residual error, and confidence intervals for parameters were not available, limiting the robustness of interpretation. Succinic acid data were not successfully modeled using conventional ATRP composites, and no reliable fits were obtained across the tested isotherm models. This may reflect poor interaction between the polar dicarboxylic acid and the more disordered polymer surface, or insufficient surface functionality to support measurable uptake.

Table 10: Fitted parameters for conventional ATRP.

	Fitted Parameter	BA	DPA	SA
Langmuir	Q_0 (mg/g)	42.7	3.01	-
	K_L (L/mg)	0.0413	$6.61 \cdot 10^{44}$	-
Freundlich	K_F (mg/g)	2.48	3.01	-
	n	1.47	1.04E25	-
Sips	Q_{ms} (mg/g)	1.58E7	3.00	-
	K_s (L/mg) $^{\beta s}$	$2.96 \cdot 10^{-5}$	$2.68 \cdot 10^{7}$	-
	β_s	0.684	1.00	-
D-R	Q_m (mg/g)	16.1	0.931	-
	β (mol^2/kJ^2)	1.47	-27.4	-

To support robust model interpretation, inclusion of comprehensive isotherm fitting data, such as those compiled in Table 9 and Table 10, are essential. While adjusted R^2 values provide a general measure of fit, they must be interpreted alongside AICc, residual error, and parameter stability. In this dataset, AICc values clearly favored the Sips model for BA and the D-R model for DPA, reinforcing their selection as best fits. However, the absence of confidence intervals for fitted parameters limits statistical rigor and prevents full evaluation of model reliability. Future work should incorporate bootstrapping or error propagation techniques to quantify uncertainty and ensure reproducibility, particularly in systems with convergence challenges or high residuals.

4.3.3.2 ARGET–ATRP Composites

ARGET-ATRP-modified composites demonstrated pronounced surface heterogeneity attributable to lower PAM brush densities and dispersed polymer coverage (Table 7). Among the tested models, the D-R fit for BA was superior, with an adjusted R^2 of 0.980 and an AICc of 4.88 (Table 9). The maximum adsorption capacity (q_m) extracted from the D-R fit was 12.541 mg/g, reflecting low absolute uptake consistent with partial monolayer development. However, the significant D-R β value of 62.897 mol^2/kJ^2 confirms strong binding energy variation, indicative of dual equilibrium behavior. This S-shaped isotherm could be interpreted by a two-stage mechanism: (1) BA binds to bare activated carbon domains, enabled by π–π stacking and/or hydrogen bonding. (2) Adsorption extends to polymer brush segments, particularly flexible regions that stabilize solute interactions via interchain association or polar interactions.[99] Or alternatively, that the adsorbate is experience adsorbate-absorbate interactions which lead to two equilibria.

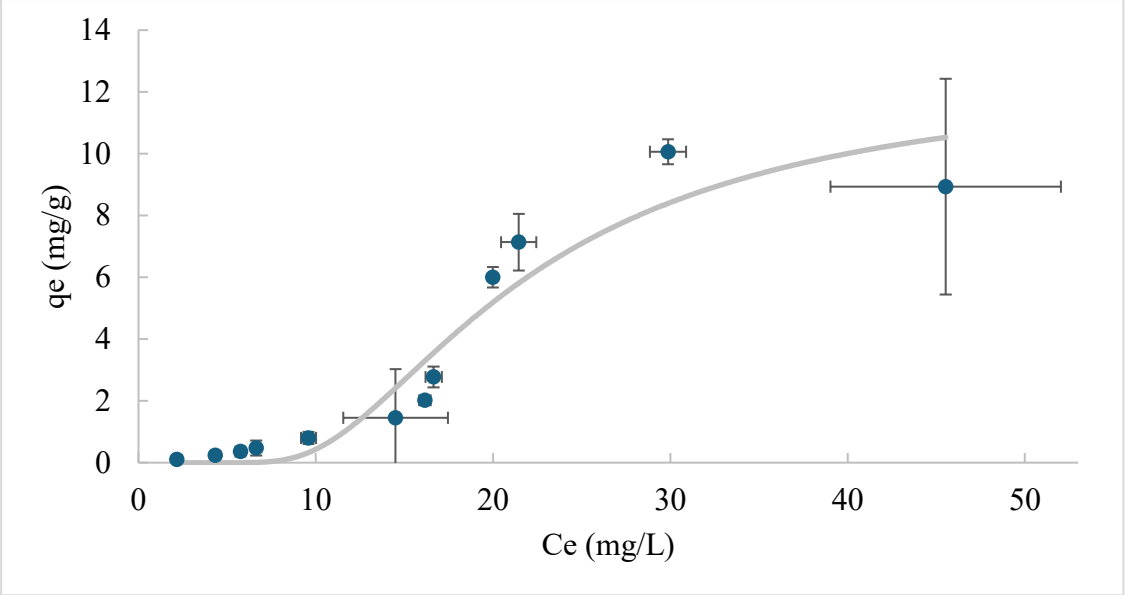

Figure 12: Isotherm model fits for BA on ARGET Composite. Modelled using D-R.

Poorly fitting models such as Langmuir and Sips, which predicted unrealistically high capacities (Q_0 = 32800 mg/g, Q_{ms} = 573 mg/g), were excluded from interpretation due to their lack of physical plausibility.

Table 11: Fitted parameters for ARGET-ATRP.

	Fitted Parameter	BA	DPA	SA
Langmuir	Q_0 (mg/g)	$3.28 \cdot 10^5$	118	0.0420
	K_L (L/mg)	$2.06 \cdot 10^6$	$1.11 \cdot 10^{-4}$	0.0319
Freundlich	K_F (mg/g)	0.00133	$1.32 \cdot 10^{-4}$	0.0100
	n	0.342	0.547	1.31
Sips	Q_{ms} (mg/g)	573	118	0.0484
	K_s (L/mg)	0.00129	$1.32 \cdot 10^{-4}$	0.0352
	β_s	1.00	1.00	0.774
D-R	Q_m (mg/g)	12.5	$1.35 \cdot 10^4$	0.0136
	β (mol^2/kJ^2)	62.9	$1.82 \cdot 10^4$	736

DPA adsorption followed a similar pattern, with the D-R model yielding R^2 = 0.850 and an AICc value of 1.51, again outperforming other models. The Q_m value of 1350 mg/g appears high but is consistent with the equilibrium capacities predicted by Langmuir (Q_0 = 32800 mg/g) and Sips (Q_{ms} = 118 mg/g) models.. The β value of 1820 mol^2/kJ^2 suggests substantial energetic heterogeneity, likely due to DPA's bulk and hydrophobicity interacting with both carbon domains and polymer brush segments. The Freundlich model, while returning n = 0.34195, was not the best fit and should not be used to infer multilayer adsorption. Similarly, Langmuir and Sips models produced exaggerated binding coefficients (KL = 0.00011, Ks = 0.00013) and were mom physical values.

For succinic acid (SA), the best-fitting model was Langmuir, with an adjusted R^2 of 0.959 and an AICc of 8 (Table 9). The Q_0 value of 0.0420 mg/g and KL of 0.0319 L/mg suggest low uptake consistent with monolayer adsorption on a relatively uniform surface.

4.3.3.3 SARA–ATRP Composites

SARA–ATRP-modified composites were distinguished by their high molecular weight PAM brushes (Mn ≈ 5.2 kg/mol) and narrow dispersity (Đ ≈ 1.25), indicative of a tightly controlled polymerization process. These characteristics favor the development of a dense, homogeneously grafted polymer layer, which restricts substrate exposure and promotes site-specific adsorption primarily within the upper brush region. This architecture markedly influences adsorption behavior, particularly favoring models that assume uniform surface properties.

For benzoic acid (BA), the Langmuir and Sips models both produced strong fits, with adjusted R^2 values of 0.919 and 0.910, respectively, and nearly identical

capacity estimates (Q_0 = 13.8 mg/g, Q_m = 13.8 mg/g). These values are consistent with the experimental qe data, which peaked around 10–12 mg/g, confirming that both models are physically plausible. The Langmuir K_L value of 0.246 L/mg suggests moderate binding affinity, likely driven by π–π stacking and hydrogen bonding with accessible amide groups. The Sips model, with β = 1, did not enhance interpretive value beyond Langmuir's ideal site coverage, though it offered a slightly better physical fit in Figure 13.

The Freundlich model returned K_F = 3.08 mg/g and n = 1.96, indicating favourable adsorption across heterogeneous sites. However, its adjusted R^2 was lower (0.85542) and AICc higher than Langmuir and Sips, suggesting it was not the best model for this system. The D-R model, while viable (Adj R^2 = 0.885), predicted a lower capacity (Q_m = 9.33 mg/g) and a β value of 0.63305 mol^2/kJ^2, indicating limited energetic diversity. Given that the Q_m value is reasonably close to experimental maxima, the D-R model may still offer insight into micropore contributions, but Langmuir remains the most appropriate model for interpretation.

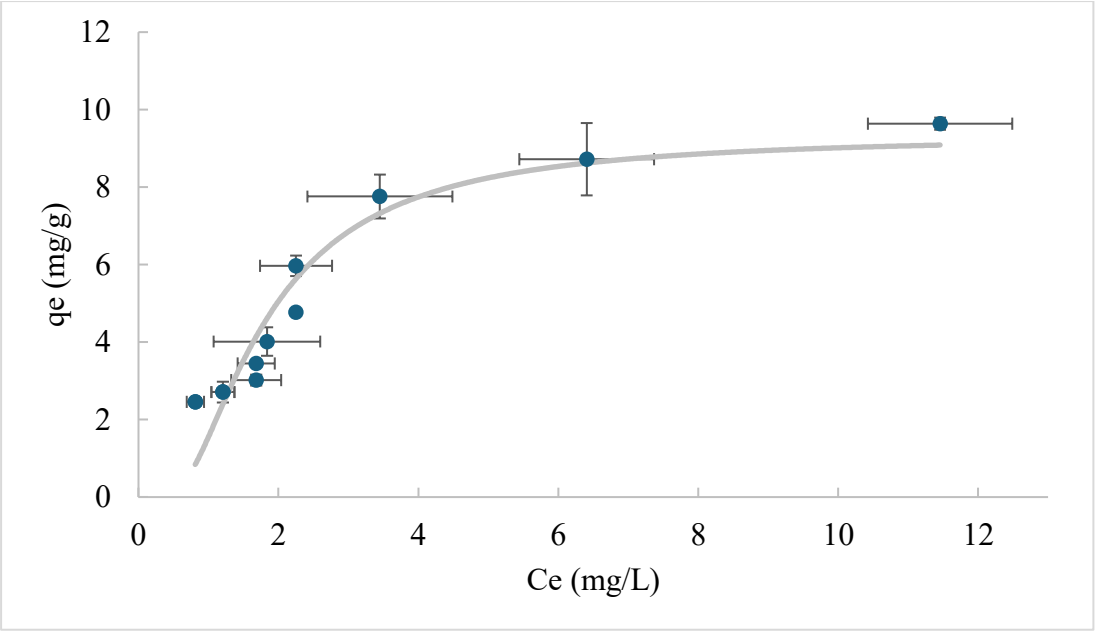

Figure 13: Model fit for BA on SARA-ATRP composites. Modelled using D-R

For DPA, only the D-R model provided a statistically viable fit, with an adjusted R^2 of 0.491 and Q_m = 4.07 mg/g. Although the β value of 395 mol^2/kJ^2 suggests significant energetic heterogeneity, the low R^2 and high residual error indicate limited confidence in the model. Langmuir, Sips, and Freundlich models failed to converge or returned unstable parameters, likely due to poor compatibility between DPA's bulky structure and the compact brush morphology of SARA-ATRP composites. This outcome supports the hypothesis that the dense, gel-like architecture of SARA-ATRP composites excludes bulky aromatic solutes like DPA from meaningful interaction, a consequence of both steric exclusion and reduced mobility within the polymer matrix. The limited accessibility of binding sites and restricted diffusion pathways likely prevent DPA from engaging in sustained adsorption, resulting in low uptake and poor model performance.

Succinic acid, despite its small size and polarity, also showed minimal adsorption on SARA-ATRP composites. The Langmuir model provided the best fit (Adj R^2 = 0.674, Q_0 = 0.0420 mg/g), consistent with low uptake and uniform site interaction. Given the low capacity and poor fit, this model should not be used for interpretation. The Freundlich and Sips models also returned low capacities and poor fits, reinforcing the conclusion that SA interacts weakly with the densely grafted surface. Despite its compact structure, SA's hydrophilicity and charge distribution may hinder uptake into the brush layer. Moreover, the brush morphology demonstrates mild gelation behavior in aqueous media, which likely leads to hydration-induced swelling and dynamic exclusion of polar solutes such as SA.[100,101]

Table 12: Fitted parameters for SARA-ATRP.

	Fitted Parameter	BA	DPA	SA
Langmuir	Q_0 (mg/g)	13.8	2.69	0.0420
	K_L (L/mg)	0.245	$-1.92 \cdot 10^{44}$	0.0319
Freundlich	K_F (mg/g)	3.08	2.69	0.0100
	n	1.96	$7.24 \cdot 10^{20}$	1.31
Sips	Q_{ms} (mg/g)	13.8	2.06	0.0484
	K_s (L/mg)	0.245	$6.13 \cdot 10^{5}$	0.0352
	β_s	1.00	0.974	0.774
D-R	Q_m (mg/g)	9.32	4.07	0.0136
	β (mol^2/kJ^2)	0.633	395	736

4.3.4 After Flocculation

Effective remediation of OSPW requires flocculants that not only enhance sedimentation but also actively reduce dissolved contaminants. In this study, both conventional PAM and AC-PAM composites were evaluated for their ability to remove key constituents from OSPW, including dissolved metals and residual polymers. By comparing post-treatment concentrations of aluminum, iron, and free polyacrylamide, the results highlight the enhanced performance of AC-PAM composites at reduced dosages. This approach demonstrates the synergistic benefits of combining carbon adsorption with polymer-driven flocculation for more efficient and environmentally responsible tailings water treatment.

Table 13: Residual adsorbates after flocculation.

Adsorbate	Sample	OSPW (ppm)	Post-flocculation (ppm)
Aluminum	0.45 wt% PAM	2.4 ± 0.7	0.10 ± 0.07
	0.25 wt% AC-PAM		0.12
Iron	0.45 wt% PAM	1.2 ± 0.8	<0.2
	0.25 wt% AC-PAM		<0.2
Polyacrylamide	0.45 wt% PAM	0.5 ± 0.7	<1
	0.25 wt% AC-PAM		<1

This expanded dataset reinforces the dual functionality of AC-PAM composites for both flocculation and contaminant adsorption. Compared to conventional PAM treatment (0.45 wt%), AC-PAM at a lower dosage (0.25 wt %) achieved comparable reductions in aluminium (0.12 ppm vs. 0.10 ± 0.07 ppm) and iron (< 0.2 ppm), indicating efficient metal capture despite decreased polymer mass. Additionally, residual polyacrylamide concentrations were < 1 ppm in both treatments, demonstrating effective separation and minimizing secondary contamination.

4.4 Conclusion

This chapter explores the adsorption performance of AC-PAM composites designed for dual functionality in oil sands tailings remediation. Building upon the flocculation results of Chapter 3, this study focuses on the physicochemical interactions between polymer brush-modified carbon substrates and model organic contaminants in OSPW.

Using batch adsorption experiments and equilibrium modelling, the chapter demonstrates that the composite's performance is intricately governed by both surface

architecture, determined by the polymerization technique, and the chemical characteristics of target analytes. Composites synthesized via controlled radical polymerization methods, ARGET-ATRP and SARA-ATRP, consistently outperformed conventional ATRP systems. Benzoic acid (BA) removal exceeded 90 % with ARGET and SARA composites, compared to less than 50 % removal using conventional ATRP, which suffered from poor dispersity and collapsed surface aggregates that hindered solute accessibility.

Isotherm modelling further reinforced these observations. ARGET composites fit best with the D-R models ($R^2 > 0.98$), capturing multilayer adsorption and site heterogeneity consistent with disordered brush architectures. D-R parameters indicated varied adsorption energies, with contributions from π–π stacking, hydrogen bonding, and van der Waals interactions. The success of the D-R model aligns with behaviours seen in molecularly imprinted polymers (MIPs), suggesting analogous heterogeneity and binding complexity.[102] In contrast, SARA-ATRP composites conformed more closely to the Langmuir and Sips models, with BA adsorption yielding $R^2 \approx 0.93$. These models displayed monolayer coverage and uniform site energy, consistent with the dense grafting and ordered morphology of the SARA brushes. However, their applicability diminished for larger solutes like DPA and highly polar species like SA, both of which showed limited interaction due to restricted access and hydration-induced exclusion from gel-like brush domains.

Looking ahead, future work should investigate hybrid isotherm models (e.g., Redlich–Peterson, Hills) to better capture nonideal adsorption behaviour, particularly for systems with intermediate site uniformity. Chemical tuning of the brush phase, through grafting of functional moieties such as carboxyl, sulfonic, or hydrophobic groups, could further enhance target selectivity. Finally, scaling to continuous

treatment systems will require transport modelling approaches, including axial dispersion and breakthrough curve analysis, especially for composites exhibiting cooperative or nonlinear adsorption dynamics.

5. Conclusions

5.1 General Conclusions

This research uses petroleum coke, an abundant waste byproduct in Alberta's bitumen upgrading process, the study proposed a sustainable route toward generating AC capable of supporting surface-initiated polymerization. The overarching goal was to evaluate petcoke's viability as an alternative substrate and to optimize polymer brush architectures via different atom transfer radical polymerization techniques, namely, conventional ATRP, ARGET-ATRP, and SARA-ATRP. These composites were then evaluated for their performance in flocculating mature fine tailings and adsorbing model contaminants from oil sands process-affected water.

The thesis first addresses the synthesis and performance of PAM brushes grafted onto both petcoke and AC substrates using various ATRP methods. SARA-ATRP produced the highest molecular weights (Mn ≈ 5.2 kg/mol) with the narrowest dispersity (Đ ≈ 1.25), resulting in dense and uniform brush architectures. ARGET-ATRP composites achieved moderate molecular weights (Mn ≈ 1.7 kg/mol) and comparable control, whereas conventional ATRP yielded polydisperse polymers (Đ > 2) that collapsed into surface aggregates. Flocculation experiments using 5 wt % MFT revealed that SARA-ATRP composites exhibited superior sedimentation rates, lower capillary suction times, reduced turbidity, and improved final solids content—even at reduced dosages compared to conventional PAM. These results confirmed that polymer brush morphology and architecture significantly influence flocculation efficiency. Post-flocculation analyses further showed that AC-PAM composites effectively removed dissolved aluminum, iron, and residual PAM from treated OSPW, demonstrating synergistic performance in contaminant removal and sedimentation.

These findings validated the dual functionality of the composite materials and showcased their promise in integrated tailings treatment.

Next the composite material was tested for its adsorption behavior, using batch experiments to assess uptake of benzoic acid, diphenyl acetic acid, and succinic acid. Composites synthesized via ARGET and SARA-ATRP displayed significantly higher BA removal (> 90 %) compared to those produced via conventional ATRP (< 50 %), a trend directly linked to their controlled polymer brush structures. ARGET and SARA brushes maintained greater functional group accessibility due to their uniform orientation and minimal chain entanglement, whereas conventional ATRP composites suffered from collapsed polymer networks. Kinetic experiments over 360 hours revealed adsorption trends highly dependent on analyte structure. SA and BA showed similar uptake (~60-65 %) due to favorable size and polarity, while DPA, a bulky aromatic compound, was restricted by steric hindrance and exhibited the lowest adsorption efficiency (~38 %).

Equilibrium isotherm modeling supported these mechanistic interpretations. ARGET-ATRP composites best fit the Dubinin–Radushkevich models, indicating multilayer adsorption on energetically heterogeneous surfaces. These findings were consistent with ARGET's disordered brush architecture and presence of accessible pore domains. SARA-ATRP composites aligned most closely with Langmuir and Sips models, suggesting monolayer adsorption on uniform sites, attributed to their tightly packed and homogeneously grafted PAM brushes. However, for larger solutes like DPA and highly polar molecules like SA, these models failed to provide reliable predictions. The composite materials thus demonstrated an effective combination of flocculation and adsorption performance, enhanced by ATRP technique and polymer architecture. Petcoke, in particular, proved to be a viable substrate, offering

comparable initiator attachment and polymer grafting efficiency to commercial AC, while reducing material cost and promoting industrial reuse.

Looking ahead, future work should focus on expanding adsorption models to better capture the behaviors observed in complex composite materials. Hybrid isotherm models such as Redlich-Peterson or Tóth can help accommodate systems with intermediate adsorption characteristics or mixed-mode binding. The brush chemistry may be optimized further through copolymerization or incorporation of polar functional groups (e.g., carboxyl, sulfonic, hydrophobic moieties) to enhance selectivity toward specific contaminants. Incorporating block copolymer architectures or gradient brush designs could improve surface accessibility while maintaining mechanical stability. Additionally, transitioning from batch to continuous flow systems will require modeling techniques that account for axial dispersion, breakthrough curves, and system kinetics under real-world conditions.

In conclusion, this work presents a novel class of dual-function composites synthesized via controlled polymerization on petcoke-derived substrates, offering a scalable, sustainable, and highly efficient solution for MFT management and OSPW remediation. The integration of flocculation and adsorption capabilities within a single, tunable platform opens new possibilities for environmental materials science and establishes a strong foundation for future industrial deployment.

5.2 Future Work

1. Investigate how polymer brush architecture (e.g., chain length, grafting density, dispersity) influences adsorption mechanisms using advanced surface

characterization tools (e.g., AFM, TEM, ellipsometry, DLS). Correlate these features with adsorbate size, polarity, and functional groups.

2. Synthesize block or hydrolyze polymer ends (e.g., PAM-co-PAA, PAM-co-PS) via ARGET–ATRP and SARA-ATRP to introduce tunable hydrophilic/hydrophobic balance or specific functional groups (e.g., amine, sulfonic acid) for selective adsorption of diverse OSPW contaminants.
3. Evaluate the recyclability of AC–PAM and P-BiBB composites through controlled desorption (e.g., pH, ionic strength, solvent treatments) and multicycle adsorption testing to assess material longevity and fouling resistance.
4. Improve petcoke activation and initiator anchoring efficiency through controlled oxidation (e.g., ozone, nitric acid) and coupling chemistry, aiming for reproducible initiator density and enhanced polymer growth kinetics.

5.3 Contributions to Science

5.3.1 Conferences

- Poster presentation at the Canadian Chemistry Conference 2024.
- MACRO polymer conference at Warwick University as of July 2024.
- Attend CSC 2025 and 9th Annual IIES Science & Policy Workshop
- Poster presentation at the Canadian Chemistry Conference 2025.

References

(1) State of Fluid Tailings Management for Mineable Oil Sands, 2023.

(2) Arslan, M.; Usman, M.; Gamal El-Din, M. Metal Sulfides in Aged-Coarse Sands Tailings Facilitate Naphthenic Acids Removal from Oil Sands Process Water. *Water Res.* **2025**, *276*, 123253.

(3) Zubot, W. Removal of Naphthenic Acids from Oil Sands Process Water Using Petroleum Coke. *Univ. Alta.* **2011**.

(4) Scott, A. C.; Zubot, W.; Davis, C. W.; Brogly, J. Bioaccumulation Potential of Naphthenic Acids and Other Ionizable Dissolved Organics in Oil Sands Process Water (OSPW) – A Review. *Sci. Total Environ.* **2020**, *712*, 134558.

(5) Li, C.; Fu, L.; Stafford, J.; Belosevic, M.; Gamal El-Din, M. The Toxicity of Oil Sands Process-Affected Water (OSPW): A Critical Review. *Sci. Total Environ.* **2017**, *601–602*, 1785–1802.

(6) Pinzón-Espinosa, A.; Kanda, R. Naphthenic Acids Are Key Contributors to Toxicity of Heavy Oil Refining Effluents. *Sci. Total Environ.* **2020**, *729*, 138119.

(7) Wang, D.; Wang, D.; Tan, X.; Yeung, A.; Liu, Q. A Review of the Roles of Constituent Minerals and Residual Bitumen in the Solid-Liquid Separation of Oil Sands Tailings. *J. Hazard. Mater.* **2023**, *451*, 131178.

(8) Omotoso, O. Prediction of Fine Tailings Settlement in Pit Lakes Using a Population Growth Model. *Environ. Geotech.* **2024**, *11* (3), 205–216.

(9) Shafaei, F.; Doulati Ardejani, F.; Bahroudi, A.; Hoseini, M.; Khakpour, M. Mechanical-Electrical Dewatering (EDW) of Mine Tailings: Influence of Voltage Level on Water Recovery and Moisture Reduction. *Miner. Eng.* **2022**, *175*, 107303.

(10) Worch, E. *Adsorption Technology in Water Treatment: Fundamentals, Processes, and Modeling*; De Gruyter: Berlin, 2012.

(11) Quinlan, P. J.; Tam, K. C. Water Treatment Technologies for the Remediation of Naphthenic Acids in Oil Sands Process-Affected Water. *Chem. Eng. J.* **2015**, *279*, 696–714.

(12) Edraki, M.; Baumgartl, T.; Manlapig, E.; Bradshaw, D.; Franks, D. M.; Moran, C. J. Designing Mine Tailings for Better Environmental, Social and Economic Outcomes: A Review of Alternative Approaches. *J. Clean. Prod.* **2014**, *84*, 411–420.

(13) *Efficient Use of Water in Tailings Management: New Technologies and Environmental Strategies for the Future of Mining*. https://www.mdpi.com/2073-4441/14/11/1741 (accessed 2025-07-09).

(14) Richardson, P. F.; Connelly, L. J. Industrial Coagulants and Flocculants. In *Reagents in Mineral Technology*; Routledge, 1988.

(15) Lin, D.; Yan, Z.; Tang, X.; Wang, J.; Liang, H.; Li, G. Inorganic Coagulant Induced Gypsum Scaling in Nanofiltration Process: Effects of Coagulant Concentration, Coagulant Conditioning Time and Fouling Strategies. *Sci. Total Environ.* **2019**, *670*, 685–695.

(16) Hamraoui, L.; Bergani, A.; Ettoumi, M.; Aboulaich, A.; Taha, Y.; Khalil, A.; Neculita, C. M.; Benzaazoua, M. Towards a Circular Economy in the Mining Industry: Possible Solutions for Water Recovery through Advanced Mineral Tailings Dewatering. *Minerals* **2024**, *14* (3), 319.

(17) Wang, C.; Harbottle, D.; Liu, Q.; Xu, Z. Current State of Fine Mineral Tailings Treatment: A Critical Review on Theory and Practice. *Miner. Eng.* **2014**, *58*, 113–131.

(18) Gregory, J.; O'Melia, C. R. Fundamentals of Flocculation. *Crit. Rev. Environ. Control* **1989**, *19* (3), 185–230.

(19) Saxena, K.; Brighu, U. Comparison of Floc Properties of Coagulation Systems: Effect of Particle Concentration, Scale and Mode of Flocculation. *J. Environ. Chem. Eng.* **2020**, *8* (5), 104311.

(20) Chakraborty, S.; Sardar, S.; Bandyopadhyay, A. Flocculation of Waste Water Using Architectural Copolymers: Recent Advancement and Future Perspective. In *Functional Polymer Nanocomposites for Wastewater Treatment*; Hato, M. J., Sinha Ray, S., Eds.; Springer International Publishing: Cham, 2022; pp 89–113.

(21) Abbasi Moud, A. Polymer Based Flocculants: Review of Water Purification Applications. *J. Water Process Eng.* **2022**, *48*, 102938.

(22) *Sweep flocculation as a second form of charge neutralisation—a review: Desalination and Water Treatment: Vol 44, No 1-3*. (accessed 2025-07-09).

(23) Gregory, J.; Barany, S. Adsorption and Flocculation by Polymers and Polymer Mixtures. *Adv. Colloid Interface Sci.* **2011**, *169* (1), 1–12.

(24) Wong, S. S.; Teng, T. T.; Ahmad, A. L.; Zuhairi, A.; Najafpour, G. Treatment of Pulp and Paper Mill Wastewater by Polyacrylamide (PAM) in Polymer Induced Flocculation. *J. Hazard. Mater.* **2006**, *135* (1), 378–388.

(25) Zeng, Y.; Yang, C.; Zhang, J.; Pu, W. Feasibility Investigation of Oily Wastewater Treatment by Combination of Zinc and PAM in Coagulation/Flocculation. *J. Hazard. Mater.* **2007**, *147* (3), 991–996.

(26) Statistics Canada. Supply and Disposition of Refined Petroleum Products, 2019. https://www150.statcan.gc.ca/n1/daily-quotidien/190315/dq190315b-eng.htm.

(27) Ren, Y.; Zheng, J.; Xu, Z.; Zhang, Y.; Cao, Z. Effect of Petcoke on the Physical-Chemical Properties of Lignite under Microwave Pyrolysis and Its Moisture Re-Adsorption Capacity. *Fuel* **2019**, *250*, 1–7.

(28) Goyal, M.; Bansal, R. C. *Activated Carbon Adsorption*, 1st ed.; CRC Press.

(29) Strong, O. K. L.; Nazari, E.; Roy, T.; Scotland, K.; Pede, P. R.; Vreugdenhil, A. J. Transforming Micropores to Mesopores by Heat Cycling KOH Activated Petcoke for Improved Kinetics of Adsorption of Naphthenic Acids. *Heliyon* **2023**, *9* (2).

(30) Eskandari, P.; Abousalman-Rezvani, Z.; Roghani-Mamaqani, H.; Salami-Kalajahi, M.; Mardani, H. Polymer Grafting on Graphene Layers by Controlled Radical Polymerization. *Adv. Colloid Interface Sci.* **2019**, *273*, 102021.

(31) Zoppe, J. O.; Ataman, N. C.; Mocny, P.; Wang, J.; Moraes, J.; Klok, H.-A. Surface-Initiated Controlled Radical Polymerization: State-of-the-Art, Opportunities, and Challenges in Surface and Interface Engineering with Polymer Brushes. *Chem. Rev.* **2017**, *117* (3), 1105–1318.

(32) Purohit, P.; Bhatt, A.; Mittal, R. K.; Abdellattif, M. H.; Farghaly, T. A. Polymer Grafting and Its Chemical Reactions. *Front. Bioeng. Biotechnol.* **2023**, *10*.

(33) Fromel, M.; Benetti, E. M.; Pester, C. W. Oxygen Tolerance in Surface-Initiated Reversible Deactivation Radical Polymerizations: Are Polymer Brushes Turning into Technology? *ACS Macro Lett.* **2022**, *11* (4), 415–421.

(34) Murad Bhayo, A.; Yang, Y.; He, X. Polymer Brushes: Synthesis, Characterization, Properties and Applications. *Prog. Mater. Sci.* **2022**, *130*, 101000.

(35) Bousquet, A.; Awada, H.; Hiorns, R. C.; Dagron-Lartigau, C.; Billon, L. Conjugated-Polymer Grafting on Inorganic and Organic Substrates: A New Trend in Organic Electronic Materials. *Prog. Polym. Sci.* **2014**, *39* (11), 1847–1877.

(36) N. K., Mays, J. W., Eds.; De Gruyter: Berlin Boston, *Reversible Deactivation Radical Polymerization: Synthesis and Applications of Functional Polymers*; Singha, **2020**.

(37) Zhao, B.; Brittain, W. J. Polymer Brushes: Surface-Immobilized Macromolecules. *Prog. Polym. Sci.* **2000**, *25* (5), 677–710.

(38) de Vos, W. M.; Kleijn, J. M.; de Keizer, A.; Cohen Stuart, M. A. Ultradense Polymer Brushes by Adsorption. *Angew. Chem.* **2009**, *121* (29), 5473–5475.

(39) Matyjaszewski, K. Atom Transfer Radical Polymerization (ATRP): Current Status and Future Perspectives. *Macromolecules* **2012**, *45* (10), 4015–4039.

(40) Krys, P.; Matyjaszewski, K. Kinetics of Atom Transfer Radical Polymerization. *Eur. Polym. J.* **2017**, *89*, 482–523.

(41) Jones, G. R.; Wang, H. S.; Parkatzidis, K.; Whitfield, R.; Truong, N. P.; Anastasaki, A. Reversed Controlled Polymerization (RCP): Depolymerization from Well-Defined Polymers to Monomers. *J. Am. Chem. Soc.* **2023**, *145* (18), 9898–9915.

(42) Jr, W. D. C.; Rethwisch, D. G. *Materials Science and Engineering: An Introduction*; John Wiley & Sons, **2020**.

(43) Qiu, J.; Charleux, B.; Matyjaszewski, K. Controlled/Living Radical Polymerization in Aqueous Media: Homogeneous and Heterogeneous Systems. *Prog. Polym. Sci.* **2001**, *26* (10), 2083–2134.

(44) Fantin, M.; Isse, A. A.; Gennaro, A.; Matyjaszewski, K. Understanding the Fundamentals of Aqueous ATRP and Defining Conditions for Better Control. *Macromolecules* **2015**, *48* (19), 6862–6875.

(45) Tsarevsky, N. V.; Sumerlin, B. S. *Fundamentals of Controlled/Living Radical Polymerization*; Royal Society of Chemistry, **2013.**

(46) Zapata-González, I.; Hutchinson, R. A.; Payne, K. A.; Saldívar-Guerra, E. Mathematical Modeling of the Full Molecular Weight Distribution in ATRP Techniques. *AIChE J.* **2016**, *62* (8), 2762–2777.

(47) Boyer, C.; Corrigan, N. A.; Jung, K.; Nguyen, D.; Nguyen, T.-K.; Adnan, N. N. M.; Oliver, S.; Shanmugam, S.; Yeow, J. Copper-Mediated Living Radical Polymerization (Atom Transfer Radical Polymerization and Copper(0) Mediated Polymerization): From Fundamentals to Bioapplications. *Chem. Rev.* **2016**, *116* (4), 1803–1949.

(48) Ribelli, T. G.; Konkolewicz, D.; Pan, X.; Matyjaszewski, K. Contribution of Photochemistry to Activator Regeneration in ATRP. *Macromolecules* **2014**, *47* (18), 6316–6321.

(49) Anastasaki, A.; Nikolaou, V.; Nurumbetov, G.; Wilson, P.; Kempe, K.; Quinn, J. F.; Davis, T. P.; Whittaker, M. R.; Haddleton, D. M. Cu(0)-Mediated Living Radical Polymerization: A Versatile Tool for Materials Synthesis. *Chem. Rev.* **2016**, *116* (3), 835–877.

(50) Konkolewicz, D.; Wang, Y.; Zhong, M.; Krys, P.; Isse, A. A.; Gennaro, A.; Matyjaszewski, K. Reversible-Deactivation Radical Polymerization in the Presence of Metallic Copper. A Critical Assessment of the SARA ATRP and SET-LRP Mechanisms. *Macromolecules* **2013**, *46* (22), 8749–8772.

(51) Kwak, Y.; Magenau, A. J. D.; Matyjaszewski, K. ARGET ATRP of Methyl Acrylate with Inexpensive Ligands and Ppm Concentrations of Catalyst. *Macromolecules* **2011**, *44* (4), 811–819.

(52) Simakova, A.; Averick, S. E.; Konkolewicz, D.; Matyjaszewski, K. Aqueous ARGET ATRP. *Macromolecules* **2012**, *45* (16), 6371–6379.

(53) Konkolewicz, D.; Krys, P.; Góis, J. R.; Mendonça, P. V.; Zhong, M.; Wang, Y.; Gennaro, A.; Isse, A. A.; Fantin, M.; Matyjaszewski, K. Aqueous RDRP in the Presence of Cu0: The Exceptional Activity of CuI Confirms the SARA ATRP Mechanism. *Macromolecules* **2014**, *47* (2), 560–570.

(54) Muller, A. H. E.; Matyjaszewski, K. Controlled and Living Polymerizations: Methods and Materials.

(55) Simakova, A.; Averick, S. E.; Konkolewicz, D.; Matyjaszewski, K. Aqueous ARGET ATRP. *Macromolecules* **2012**, *45* (16), 6371–6379.

(56) Matyjaszewski, K.; Dong, H.; Jakubowski, W.; Pietrasik, J.; Kusumo, A. Grafting from Surfaces for “Everyone”: ARGET ATRP in the Presence of Air. *Langmuir* **2007**, *23* (8), 4528–4531.

(57) Jones, G. R.; Antonopoulou, M.-N.; Truong, N. P.; Anastasaki, A. Initiators for Continuous Activator Regeneration (ICAR) Depolymerization. *J. Am. Chem. Soc.* **2024**, *146* (51), 35023–35028.

(58) Krys, P.; Schroeder, H.; Buback, J.; Buback, M.; Matyjaszewski, K. The Borderline between Simultaneous Reverse and Normal Initiation and Initiators for Continuous Activator Regeneration ATRP. *Macromolecules* **2016**, *49* (20), 7793–7803.

(59) Roy, T. M.; Nazari, E.; Strong, O. K. L.; Pede, P. R.; Vreugdenhil, A. J. The Effect of Adsorbent Textural and Functional Properties on Model Naphthenic Acid Adsorption. *J. Environ. Sci.* **2025**, *148*, 27–37.

(60) Bansal, R. C.; Goyal, M. *Activated Carbon Adsorption*, First issued in paperback.; CRC Press, Taylor & Francis Group: Boca Raton London New York, **2020**.

(61) Brunauer, S.; Emmett, P. H.; Teller, E. Adsorption of Gases in Multimolecular Layers. *J. Am. Chem. Soc.* **1938**, *60* (2), 309–319.

(62) Inglezakis, V. J.; Fyrillas, M. M. Adsorption Fixed Beds Modeling Revisited: Generalized Solutions for S-Shaped Isotherms. *Chem. Eng. Commun.* **2017**, *204* (11), 1299–1317.

(63) Buttersack, C. Modeling of Type IV and V Sigmoidal Adsorption Isotherms. *Phys. Chem. Chem. Phys.* **2019**, *21* (10), 5614–5626.

(64) Butyrskaya, E. Understanding the Mechanism of Monolayer Adsorption from Isotherm. *Adsorption* **2024**, *30* (6), 1395–1406.

(65) Chu, K. H. Fitting a Little-Known Isotherm Equation to S-Shaped Adsorption Equilibrium Data. *Sep. Purif. Technol.* **2021**, *259*, 118079.

(66) Lima, É. C.; Adebayo, M. A.; Machado, F. M. Kinetic and Equilibrium Models of Adsorption. In *Carbon Nanomaterials as Adsorbents for Environmental and Biological Applications*; Bergmann, C. P., Machado, F. M., Eds.; Springer International Publishing: Cham, 2015; pp 33–69.

(67) Tran, H. N.; Thanh Trung, N. P.; Lima, E. C.; Bollinger, J.-C.; Dat, N. D.; Chao, H.-P.; Juang, R.-S. Revisiting the Calculation of Thermodynamic Parameters of Adsorption Processes from the Modified Equilibrium Constant of the Redlich–Peterson Model. *J. Chem. Technol. Biotechnol.* **2023**, *98* (2), 462–472.

(68) Limousin, G.; Gaudet, J.-P.; Charlet, L.; Szenknect, S.; Barthès, V.; Krimissa, M. Sorption Isotherms: A Review on Physical Bases, Modeling and Measurement. *Appl. Geochem.* **2007**, *22* (2), 249–275.

(69) Hutson, N. D.; Yang, R. T. Theoretical Basis for the Dubinin-Radushkevitch (D-R) Adsorption Isotherm Equation. *Adsorption* **1997**, *3* (3), 189–195.

(70) Stevie, F. A.; Donley, C. L. Introduction to X-Ray Photoelectron Spectroscopy. *J. Vac. Sci. Technol. A* **2020**, *38* (6), 063204.

(71) Engelhard, M. H.; Baer, D. R.; Herrera-Gomez, A.; Sherwood, P. M. A. Introductory Guide to Backgrounds in XPS Spectra and Their Impact on Determining Peak Intensities. *J. Vac. Sci. Technol. A* **2020**, *38* (6), 063203.

(72) Baer, D. R.; Artyushkova, K.; Cohen, H.; Easton, C. D.; Engelhard, M.; Gengenbach, T. R.; Greczynski, G.; Mack, P.; Morgan, D. J.; Roberts, A. XPS Guide: Charge Neutralization and Binding Energy Referencing for Insulating Samples. *J. Vac. Sci. Technol. A* **2020**, *38* (3), 031204.

(73) Walls, J. M.; Smith, R. *Surface Science Techniques*; Elsevier, **2013.**

(74) Wang, J.; Guo, X. Adsorption Kinetic Models: Physical Meanings, Applications, and Solving Methods. *J. Hazard. Mater.* **2020**, *390*, 122156.

(75) Bonilla-Petriciolet, A., Mendoza-Castillo, D. I., Reynel-Ávila, H. E. *Adsorption Processes for Water Treatment and Purification*;, Eds.; Springer International Publishing: Cham, **2017.**

(76) Eder, S.; Müller, K.; Azzari, P.; Arcifa, A.; Peydayesh, M.; Nyström, L. Mass Transfer Mechanism and Equilibrium Modelling of Hydroxytyrosol Adsorption on Olive Pit–Derived Activated Carbon. *Chem. Eng. J.* **2021**, *404*, 126519.

(77) Insights into the Modeling of Adsorption Isotherm Systems. *Chem. Eng. J.* **2010**, *156* (1), 2–10.

(78) Swenson, H.; Stadie, N. P. Langmuir's Theory of Adsorption: A Centennial Review. *Langmuir* **2019**, *35* (16), 5409–5426.

(79) Tran, H. N. Improper Estimation of Thermodynamic Parameters in Adsorption Studies with Distribution Coefficient KD (Qe/Ce) or Freundlich Constant (KF): Considerations from the Derivation of Dimensionless Thermodynamic Equilibrium Constant and Suggestions. *Adsorpt. Sci. Technol.* **2022**, *2022*.

(80) de Vargas Brião, G.; Hashim, M. A.; Chu, K. H. The Sips Isotherm Equation: Often Used and Sometimes Misused. *Sep. Sci. Technol.* **2023**, *58* (5), 884–892.

(81) Gil, A.; Grange, P. Application of the Dubinin-Radushkevich and Dubinin-Astakhov Equations in the Characterization of Microporous Solids. *Colloids Surf. Physicochem. Eng. Asp.* **1996**, *113* (1), 39–50.

(82) Vasanth Kumar, K.; Gadipelli, S.; Wood, B.; A. Ramisetty, K.; A. Stewart, A.; A. Howard, C.; L. Brett, D. J.; Rodriguez-Reinoso, F. Characterization of the Adsorption Site Energies and Heterogeneous Surfaces of Porous Materials. *J. Mater. Chem. A* **2019**, *7* (17), 10104–10137.

(83) Biçakci, E.; Erzengin, S. G.; Alp, F. B. Recovery of Phenylethyl Alcohol from Aqueous Solution by Batch Adsorption. *Open Chem.* **2025**, *23* (1).

(84) Freeman, E. M.; Siemieniewska, T.; Marsh, H.; Rand, B. A Critique and Experimental Observations of the Applicability to Microporosity of the Dubinin Equation of Adsorption. *Carbon* **1970**, *8* (1), 7–17.

(85) Iglesias, A. M. Treatment of Synthetic Oil Sands Tailing Water with Activated Carbon.

(86) Lawtae, P.; Tangsathitkulchai, C. A New Approach for Controlling Mesoporosity in Activated Carbon by the Consecutive Process of Air Oxidation, Thermal

Destruction of Surface Functional Groups, and Carbon Activation (the OTA Method). *Molecules* **2021**, *26* (9), 2758.

(87) Wu, Y.; Zhang, N.; De Lannoy, C.-F. Upcycling Wildfire-Impacted Boreal Peats into Porous Carbons That Efficiently Remove Phenolic Micropollutants. *J. Environ. Chem. Eng.* **2021**, *9* (4), 105305.

(88) Fisher, K. S.; Vreugdenhil, A. J. Metal-Impregnated Petroleum Coke-Derived Activated Carbon for the Adsorption of Arsenic in Acidic Waters. *ACS Omega* **2023**, *8* (32), 29083–29100.

(89) Mutlu, H.; Ceper, E. B.; Li, X.; Yang, J.; Dong, W.; Ozmen, M. M.; Theato, P. Sulfur Chemistry in Polymer and Materials Science. *Macromol. Rapid Commun.* **2019**, *40* (1), 1800650.

(90) Krys, P.; Fantin, M.; Mendonça, P. V.; Abreu, C. M. R.; Guliashvili, T.; Rosa, J.; Santos, L. O.; Serra, A. C.; Matyjaszewski, K.; Coelho, J. F. J. Mechanism of Supplemental Activator and Reducing Agent Atom Transfer Radical Polymerization Mediated by Inorganic Sulfites: Experimental Measurements and Kinetic Simulations. *Polym. Chem.* **2017**, *8* (42), 6506–6519.

(91) Hripko, R.; Vajihinejad, V.; LopesMotta, F.; Soares, J. B. P. Enhanced Flocculation of Oil Sands Mature Fine Tailings Using Hydrophobically Modified Polyacrylamide Copolymers. *Glob. Chall.* **2018**, *2* (3), 1700135.

(92) Edmondson, S.; L. Osborne, V.; S. Huck, W. T. Polymer Brushes via Surface-Initiated Polymerizations. **2004**.

(93) Barbey, R.; Lavanant, L.; Paripovic, D.; Schüwer, N.; Sugnaux, C.; Tugulu, S.; Klok, H.-A. Polymer Brushes via Surface-Initiated Controlled Radical Polymerization: Synthesis, Characterization, Properties, and Applications. *Chem. Rev.* **2009**, *109* (11), 5437–5527.

(94) Dubey, R.; Shende, P. Potential of Brush and Mushroom Conformations in Biomedical Applications. *Chem. Pap.* **2024**, *78* (12), 6873–6889. https://doi.org/10.1007/s11696-024-03602-3.

(95) Sherazi, T. A. Graft Polymerization. In *Encyclopedia of Membranes*; Springer, Berlin, Heidelberg, 2016; pp 886–887.

(96) Stokolos, O. A.; Ivanova, L. V.; Sorokin, A. S.; Koshelev, V. N. Comparative Study of the Composition and Structure of Naphthenic Acids of Crude Oil from the Naftalan and Anastasievsko-Troitskoe Fields. *Pet. Chem.* **2020**, *60* (1), 22–29.

(97) Tsuzuki, S. Interactions with Aromatic Rings. In *Intermolecular Forces and Clusters I*; Wales, D. J., Ed.; Springer: Berlin, Heidelberg, 2005; pp 149–193.

(98) Villarroel-Rocha, J.; Arroyo-Gómez, J. J.; Barrera, D.; Sapag, K. A New and Reliable Method to Obtain Micropore Volume in Nanoporous Solids by Gas Adsorption Based on Dubinin Works and the Thickness of the Adsorbed Layer. *J. Porous Mater.* **2024**, *31* (3), 1111–1120.

(99) *Surfactant Adsorption Isotherms: A Review | ACS Omega*. https://pubs.acs.org/doi/full/10.1021/acsomega.1c04661 (accessed 2025-08-13).

(100) Conrad, J. C.; Robertson, M. L. Shaping the Structure and Response of Surface-Grafted Polymer Brushes via the Molecular Weight Distribution. *JACS Au* **2023**, *3* (2), 333–343.

(101) Wang, J.; Klok, H. Swelling-Induced Chain Stretching Enhances Hydrolytic Degrafting of Hydrophobic Polymer Brushes in Organic Media. *Angew. Chem. Int. Ed.* **2019**, *58* (29), 9989–9993.

(102) Shimizu, K. D. Characterization of MIPs Using Heterogeneous Binding Models. *MRS Online Proc. Libr. OPL* **2002**, *723*, M1.4.